Tectonophysics 846 (2023) 229659

Contents lists available at ScienceDirect

Tectonophysics

journal homepage: www.elsevier.com/locate/tecto

Seismotectonic evidence for present-day transtensional reactivation of the slowly deforming Hegau-Bodensee Graben in the northern foreland of the Central Alps

Tobias Diehl [a,*], Herfried Madritsch [b,1], Michael Schnellmann [b], Thomas Spillmann [b], Elmar Brockmann [c], Stefan Wiemer [a]

[a] Swiss Seismological Service, ETH Zürich, Sonneggstrasse 5, CH-8092 Zürich, Switzerland
[b] Nagra (National Cooperative for the Disposal of Radioactive Waste), CH-5430 Wettingen, Switzerland
[c] Federal Office of Topography swisstopo, Swiss Geological Survey, Divison of Geodesy and Federal Directorate of Cadastral Surveying, Seftigenstrasse 264, CH-3084 Wabern, Switzerland

ARTICLE INFO

Keywords:
Seismicity
Focal mechanisms
Stress inversion
Geodesy
Seismic Hazard

ABSTRACT

This study presents a seismotectonic analysis of the Miocene-aged Hegau-Bodensee Graben, a major tectonic element in the northern foreland of the European Central Alps. The graben is characterized by comparatively low strain rates and low-to-moderate seismicity. Our study builds on the seismological analysis of earthquakes recorded by a recently densified seismometer network. The derived high-precision absolute and relative hypocenter relocations allow to identify seismogenic structures in the pre-Mesozoic basement, which we relate to bounding faults on either side of the NW-SE striking graben. A cluster of seismicity on the SW side of the graben is associated with the previously mapped Neuhausen Fault. In contrast, the seismogenic, SW-dipping bounding faults on the opposite side of the graben, between the extinct Hegau volcanic field and the Bodanrück peninsula of Lake Constance, cannot be associated with any known fault. A set of 51 focal mechanisms allows for a high-resolution analysis of kinematics and stress regime of the graben. Our results show that the bounding faults of the graben are optimally oriented to be reactivated in transtensional mode in the present-day stress field. Slip rates across the Neuhausen and Randen Faults estimated from geodetic data are likely <0.1 mm/yr. In comparison with historical seismicity over the past 600 years and geomorphic field observations, geodetic rates of 0.1 mm/yr appear overestimated. Nevertheless, historical seismicity suggests that slip rates have the potential to generate M_W 5.0 earthquakes within this slowly deforming, transtensional fault zone in the foreland of the Alpine collision zone on timescales of several hundred years.

1. Introduction

The seismotectonic characterization and seismic hazard assessment of low-strain, intraplate areas, typically characterized by long earthquake recurrence times and low surface deformation rates close to the noise level of modern geodetic recording capabilities, represent a seismological challenge (Landgraf et al., 2017 with references therein). Seismic activity in such settings is low to moderate and usually scattered, indicating that deformation is distributed over several fault segments rather than localized along a major fault zone. Nevertheless, these areas can still host devastating earthquakes of magnitudes $\geq$6, with recurrence intervals exceeding several thousand years. The most prominent example of such intraplate seismicity is the New Madrid Seismic Zone in the eastern United States, which is associated with the reactivation of a Precambrian rift (Braile et al., 1986). This zone hosted several M8 earthquakes between 1811 and 1812 (e.g., Johnston and Schweig, 1996) despite small (on the order of 3–5 mm/yr) to non-detectable present-day intraplate strain accumulation (e.g., Weber et al., 1998; Newman et al., 1999). Similarly, the largest historical intraplate earthquake in Central Europe, the 1356 M_W 6.7–7.1 earthquake of Basel (e.g., Meghraoui et al., 2001; Fäh et al., 2009), occurred in such a continental low-strain area. Like the entire northern foreland of

* Corresponding author.
E-mail address: tobias.diehl@sed.ethz.ch (T. Diehl).
[1] Now at: Federal Office of Topography swisstopo, Swiss Geological Survey, Seftigenstrasse 264, CH-3084 Wabern, Switzerland.

https://doi.org/10.1016/j.tecto.2022.229659
Received 23 December 2021; Received in revised form 16 November 2022; Accepted 22 November 2022
Available online 28 November 2022

the European Alps, its source region at the southern end of the Upper Rhine Graben (Fig. 1) is characterized by present-day deformation rates <1 mm/yr (e.g., Schlatter, 2007; Schlatter, 2014; Brockmann et al., 2012; Villiger, 2014; Houlie et al., 2018; Sánchez et al., 2018).

The focus of the study presented here, is the Hegau-Bodensee Graben (also referred to as Hegau-Lake Constance Graben; e.g., Fabbri et al., 2021, hereafter referred to as HBG), located about 100 km to the east of the Upper Rhine Graben (Fig. 1). The HBG is part of the larger Freiburg–Bonndorf–Bodensee Fault Zone shown in Fig. 1, which represents a major tectonic element in the northern foreland of the Central Alps (e.g., Egli et al., 2017). Although the HBG has been recognized to be seismically active at low to moderate levels previously (e.g., Deichmann et al., 2000a; Diehl et al., 2018), associated seismotectonic processes and their significance in the geodynamic context of the Alpine foreland are still poorly understood. Likewise, its relation to the seismically more active neighboring Upper Rhine Graben and the Albstadt Shear Zone (Fig. 1), along which devasting earthquakes have occurred during historical times (e.g., Bonjer et al., 1984; Deichmann et al., 2000a; Lopes Cardozo and Granet, 2003; Barth et al., 2015; Stange and Brüstle, 2005; Mader et al., 2021) is unclear. Since 1995, several earthquake swarms occurred near the cities of Singen and Constance (Fig. 1), with local magnitudes (M_L) up to 3.7, which triggered questions on driving mechanisms of these sequences and possible seismic hazard associated with the graben structure. Another feature of the Hegau-Lake Constance region, as well as the entire northern foreland of the Central Alps, is the seismic activity throughout the entire crust, including its lowermost part (e.g., Deichmann, 1992). Stresses induced by slab-rollback and crustal-delamination processes have been proposed to explain the lower-crustal seismicity in the Alpine foreland (Singer et al., 2014), however, possible links to very shallow crustal structures such as the HBG are still unclear. Given the region's dense population and the proximity to potential siting regions for deep geological nuclear waste repositories (Fig. 2; Nagra, 2008, 2014), an improved seismotectonic characterization of the HBG is being sought.

To achieve this goal, the seismological network across the region was significantly densified in order to improve the magnitude of completeness (M_C) of seismicity and the quality of earthquake locations in northern Switzerland and southern Germany over the past two decades. In this study, we make use of the data acquired by this improved network and image seismogenic faults associated with the HBG with unprecedented high-resolution hypocenter relocations. Seismicity is interpreted in combination with a recent three-dimensional (3-D) local earthquake tomography model (Diehl et al., 2021b) and geological models based on seismic reflection data. Fault kinematics and the stress regime of the graben are derived from an augmented set of focal mechanisms. Finally, upper bounds of slip rates of bounding faults are estimated from already existing Global Navigation Satellite System (GNSS) calculated velocities (Brockmann, 2018, Brockmann et al., 2019) and compared to the seismic moment release of historical and instrumentally recorded earthquakes.

2. Geological and tectonic setting

The NW-SE striking HBG lies within an area exposing the Mesozoic cover of Variscan basement, straddling the northern rim of the Molasse Basin of the European Alps approximately 50 km of the orogenic thrust

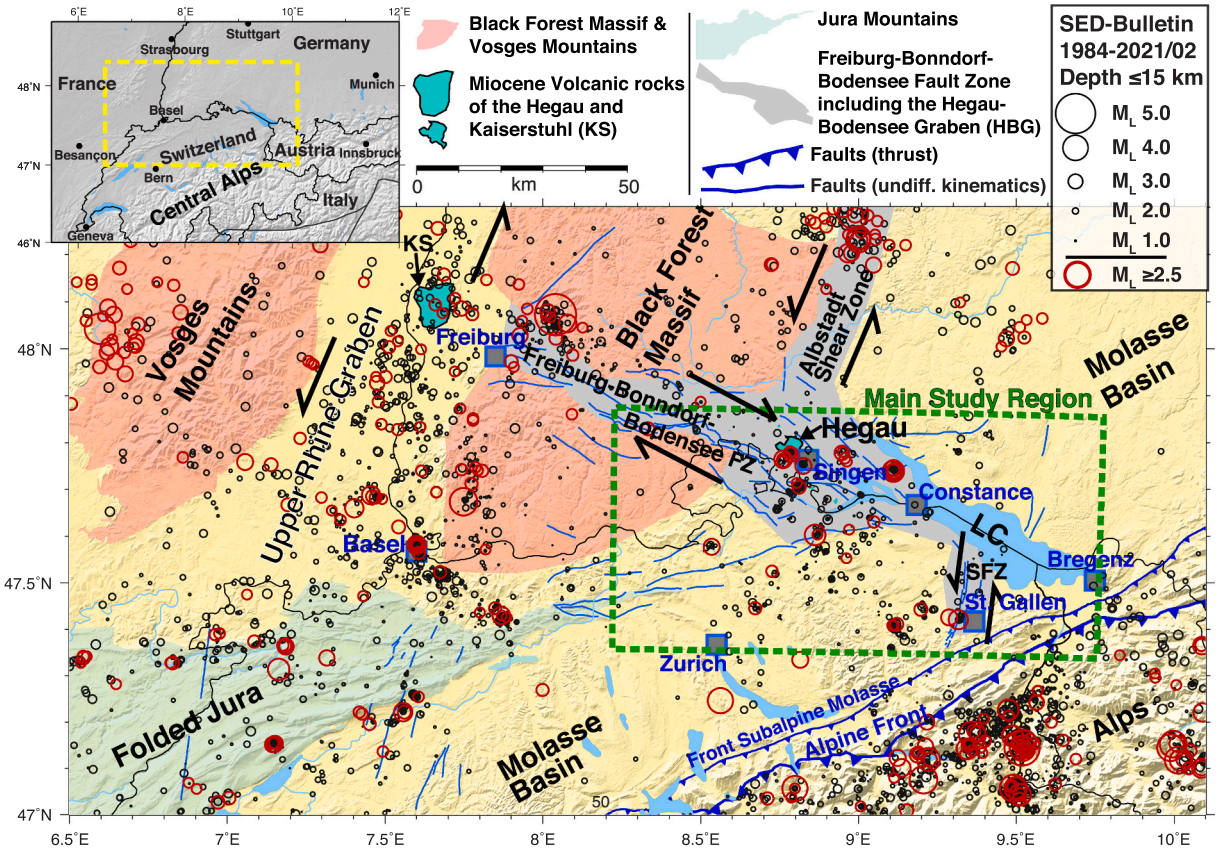

Fig. 1. Simplified tectonic map of the northern foreland of the Central Alps with upper-crustal seismicity (focal depth ≤ 15 km). Tectonic units and faults are adopted from Egli et al. (2017), Heuberger et al. (2016), Mock and Herwegh (2017) and Swisstopo (2005). Gray areas indicate major fault and shear zones, including the Hegau-Bodensee Graben (HBG). Displayed seismicity (circles) corresponds to bulletin locations of the Swiss Seismological Service (SED) in the period 1984/01–2021/02. Size of the circles indicates local magnitude (M_L). Red circles highlight earthquakes of $M_L \geq 2.5$. The green dashed line defines the main study region including the HBG. LC: Lake Constance (German: "Bodensee"); KS: Kaiserstuhl; SFZ: St. Gallen Fault Zone. (For interpretation of the references to colour in this figure legend, the reader is referred to the web version of this article.)

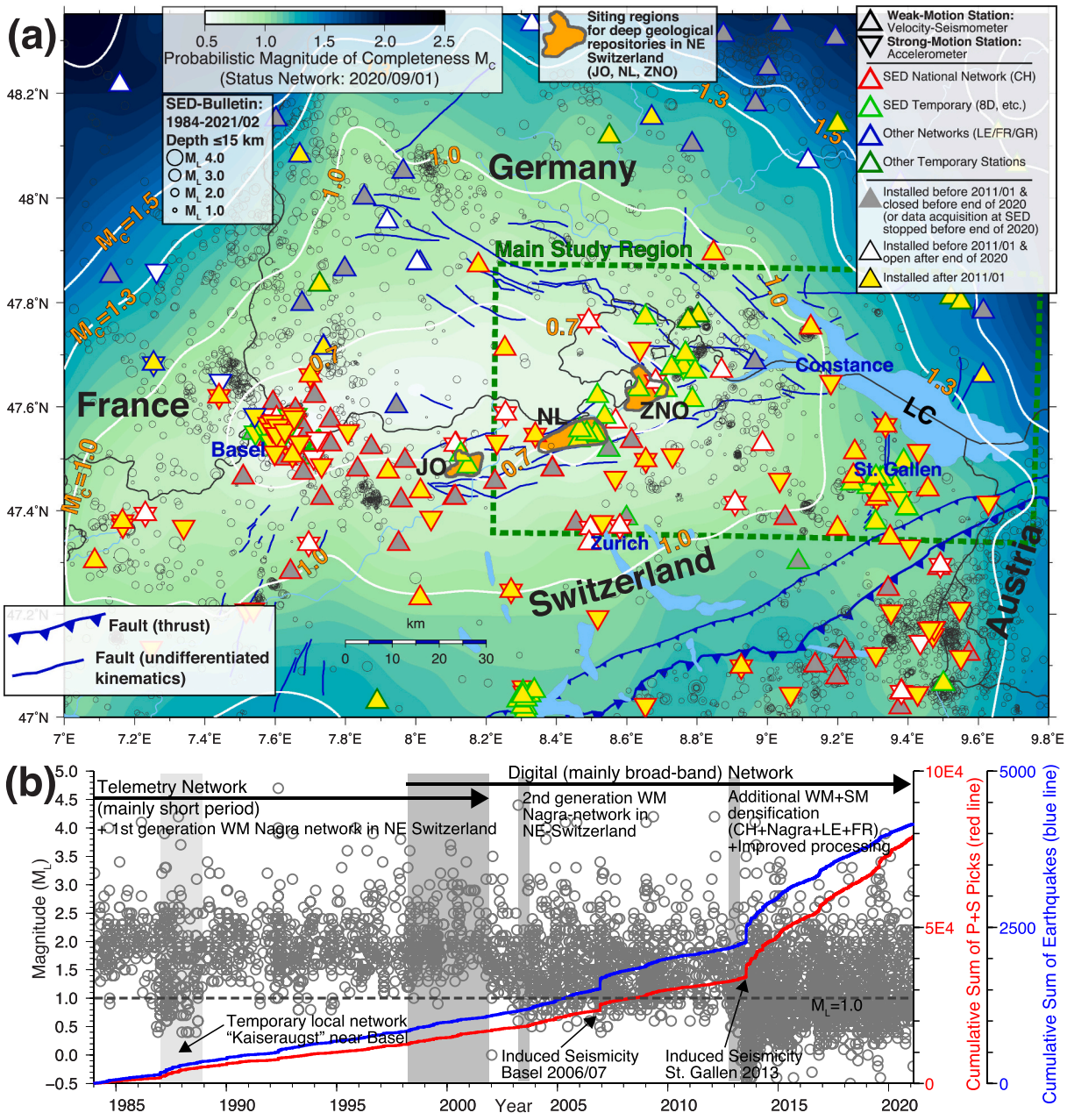

Fig. 2. Seismic network configuration, magnitude of completeness (M_C) and temporal evolution of earthquake detection capabilities in the northern foreland of the Central Alps. (a) Seismic network used in this study, including open and closed weak-motion (WM; seismometers) and strong-motion (SM; accelerometers) stations operated by various seismological agencies. The seismic network in the Hegau-Lake Constance region (outlined by green, dashed line) has been significantly improved since about 2011. Background colors and white contour lines indicate M_C estimates (in terms of local magnitude M_L) derived from the probabilistic *PMC* method (see text for details) for the network configuration as of September 2020. Circles correspond to upper-crustal seismicity of the SED earthquake bulletin. Orange areas indicate three potential siting regions for underground nuclear waste repositories (JO: Jura Ost; NL: Nördlich Lägern; ZNO: Zürich Nordost; Nagra, 2008, Nagra, 2014). Blue lines indicate faults (see caption of Fig. 1 for references of shown fault traces). LC: Lake Constance. (b) M_L as function of origin time of earthquakes located within the geographic boundaries of (a) and occurring in the digital era of SED's instrumental earthquake catalog (1984–2021/02). Blue line indicates the cumulative sum of earthquakes, red line shows cumulative sum of *P* and *S* arrival-time picks listed in the SED bulletin. Vertical gray bars indicate major changes in network configuration in the wider study area. (For interpretation of the references to colour in this figure legend, the reader is referred to the web version of this article.)

front (Fig. 1). The Molasse basin developed during Oligocene and Miocene times (Pfiffner, 1986; Willett and Schlunegger, 2010). Its sedimentary fill consists of 4 mega-sequences of clastic sediments (Homewood et al., 1986). Subjected to large-scale erosion during Late Miocene/Pliocene times (von Hagke et al., 2012), the thickness of Molasse sediments in the area of the HBG preserved today amounts to some 500 m. To the north and east, the gently south dipping Mesozoic sequence underlying the Cenozoic basin fill is exposed. It developed under epi-continental marine conditions and is dominated by limestones, marls and clays and evaporites at its base. Even further to the north in the Black Forest Massif, the crystalline basement underneath the Mesozoic is exposed. The pre-Permian granites and gneisses were strongly deformed during Variscan orogeny and later dissected by several regional fault zones including low-angle normal faults and thrusts as well steeply to subvertical strike-slip fault systems (Eisbacher et al., 1989; Madritsch et al., 2018).

In the Hegau region, the sedimentation of Molasse deposits was accompanied by volcanism during Middle and Late Miocene times (Lippolt et al., 1963; Wimmenauer, 1974; Schreiner, 1992). The volcanic field in this region coincides with the intersection of two fault zones (see Fig. 1), the N–S trending Albstadt Shear Zone (Schneider, 1979; Reinecker and Schneider, 2002; Mader et al., 2021) and the roughly NW–SE trending Freiburg–Bonndorf–Bodensee Fault Zone (Egli et al., 2017 with references therein; see further outline below). The latter fault zone is traceable for several tens of kilometers passing through the crystalline basement of the Black Forest Massif into the Upper Rhine Graben (Fig. 1) and thus represents a major crustal-scale discontinuity. The HBG represents its southeasternmost extent.

The formation of the NW-SE striking HBG investigated here, is inferred to have resulted from the transtensional to extensional reactivation of the Freiburg-Bonndorf-Bodensee Fault Zone during the Middle Miocene (Schreiner, 1992; Egli et al., 2017).

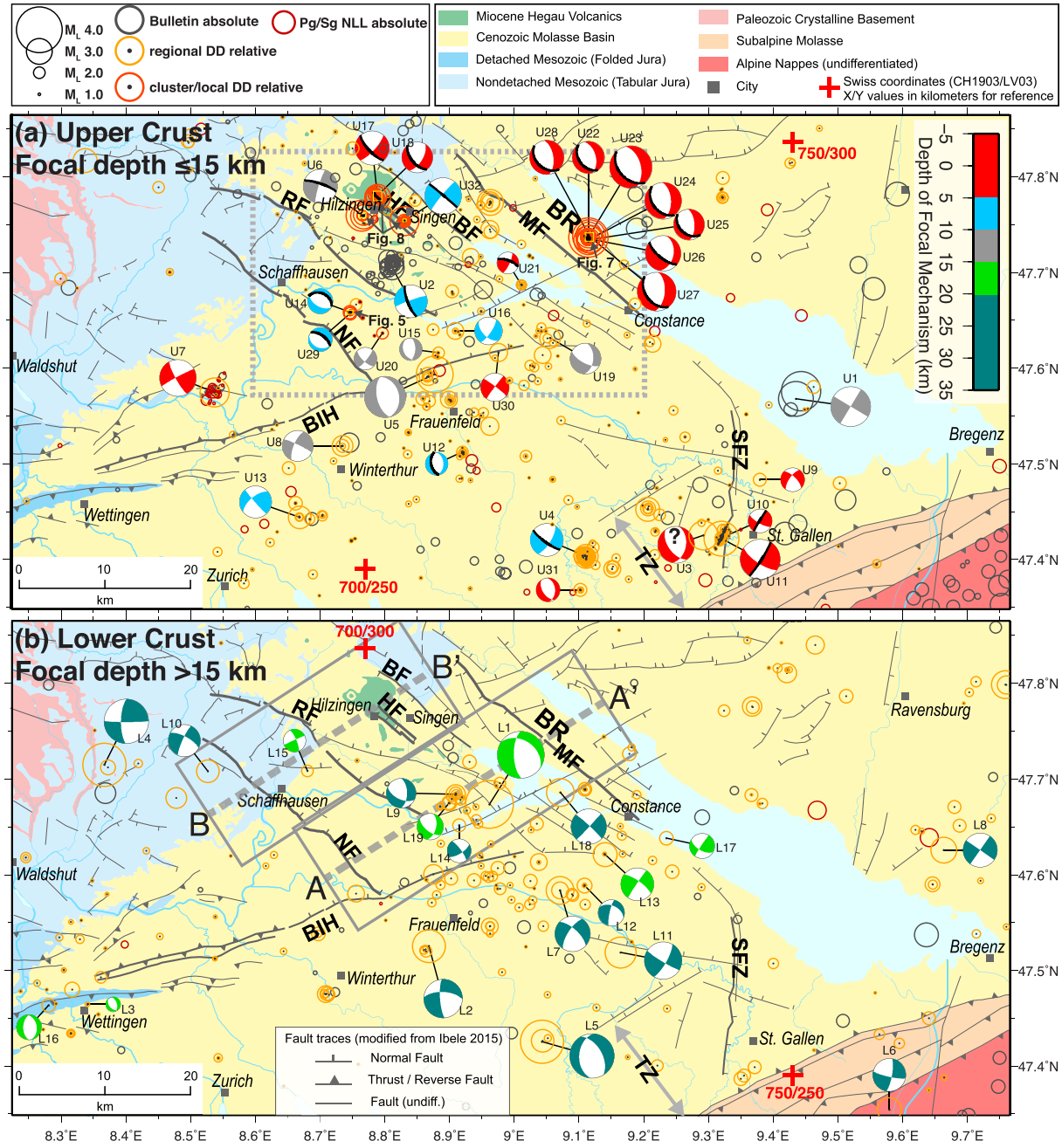

Fig. 3. Tectonic map of the Hegau-Lake Constance region with first-motion focal mechanisms (FM) and hypocenter locations of the *MERGECAT* catalog (Fig. S1) divided into two depth intervals. (a) Focal depths ≤15 km: Representing upper-crustal seismicity. Focal planes marked by bold black lines correspond to active planes determined by relative relocation of fore- and/or aftershocks. Normal-fault component of solution U3 (marked by question mark) is considered uncertain (see Diehl et al., 2017). FMs within the box outlined by the gray dashed line are used to invert for the orientation of principal stress axes in the upper crust in the Hegau-Bodensee Graben as described in Section 4.3. (b) Focal depths >15 km: Representing lower-crustal seismicity. Gray dashed lines indicate location of two vertical profiles presented in Fig. 4, with the gray boxes indicating the epicentral range of seismicity projected to the corresponding profiles. All FMs are shown as lower-hemisphere stereographic projections and colors of compressional quadrant of FMs indicate focal depth. Fault traces modified after Ibele (2015). BF: Buchberg Fault; BIH: Baden-Irchel-Herdern Fault Zone; BR: Bodanrück Peninsula; HF: Hegau Faults; MF: Mindelsee Fault; NF: Neuhausen Fault; RF: Randen Fault; SFZ: St. Gallen Fault Zone; TZ: Triangle Zone.

Geomorphologically, the 536 km^2 large Lake Constance (German: "Bodensee") is a remarkable feature that occupies a glacially overdeepened Quaternary basin (Müller and Gees, 1968; Schreiner, 1992). The fact that this basin at least partially follows the Miocene graben trend has led previous authors to suspect that the formation of the glacial basin was tectonically guided. Indeed, recent high-resolution bathymetric and reflection seismic investigations of the lake have revealed a number of faults that appear to have been active during Quaternary times (Fabbri et al., 2021). In the following, the most prominent known fault zones in the area of the HBG are briefly described (see also Fig. 3).

The roughly NW-SE striking Neuhausen Fault (NF in Fig. 3) is the westernmost fault of the HBG cropping out at the surface. It is a segmented normal fault (top to NE), whose vertical throw within the Mesozoic section is estimated to range between 20 and 50 m, locally up to 100 m (Birkhäuser et al., 2001; Roche et al., 2020). A relatively more important normal fault, also top to the NE, within the Miocene graben is the similarly striking Randen Fault (RF in Fig. 3) located farther to the east with a documented vertical throw of >200 m (Schreiner, 1992). Both faults were previously considered to have potentially been active during the Quaternary (Müller et al., 2002). Even farther to the north and northeast (e.g., within the NE part of the graben) there are a number of other NW-SE striking faults mentioned in the literature (cf. Ibele, 2015 with references therein; for example, the Hegau and Mindelsee Faults; HF and MF in Fig. 3). Their traces are generally far less constrained compared to the previously mentioned ones, but some of them seem to be traceable into the Lake Constance and may have been recently active (Fabbri et al., 2021). Apart from graben-parallel faults described above that are part of the HBG, other important fault systems in the investigated region include the ENE-WSW striking Permocarboniferous trough of northern Switzerland (Constance-Frick Trough; cf. Madritsch et al., 2018 with references therein) and the N-S striking St. Gallen Fault Zone (SFZ in Fig. 3; Heuberger et al., 2016). While there is no clear evidence for ongoing activity of the faults associated with the Constance-Frick Trough beyond their Miocene reactivation (e.g., the Baden-Irchel Herdern Lineament; BIH in Fig. 3; Malz et al., 2016), the St. Gallen Fault Zone has been found to be currently active as it offsets Quaternary sediments in Lake Constance (Fabbri et al., 2021). These geological evidences for fault activity in the Hegau-Lake Constance area are corroborated by low-to-moderate but continuous seismicity, whose improved seismotectonic analysis is the main goal of this study.

3. Data and methods

3.1. Seismological data

The Swiss Seismological Service at ETH Zurich (SED) operates single seismic stations and local seismic networks in northern Switzerland since the early 1970s (for an overview see Deichmann et al., 2000a). A particular target of the dense instrumentation in this region is the monitoring and characterization of seismicity at sites of potential nuclear waste repositories on behalf of the *National Cooperative for the Disposal of Radioactive Waste* (Nagra). Digital seismic waveforms of earthquakes recorded by the "first-generation" Nagra weak-motion networks are available from 1984 onwards. Event data acquired before the year 2002 were mainly recorded by short-period seismometers and transmitted to data centers through telemetry, resulting in a narrow dynamic range of signals (Fig. 2b; Deichmann et al., 2000a). Since the year 2002, the majority of stations operated in northern Switzerland consists of three-component, short or broad-band sensors with continuous, digital data transmission (Fig. 2b), leading to significantly improved recording quality.

In the year 2003, Nagra's "second-generation" weak-motion network, consisting of five stations, finally replaced the "first-generation" stations. Since about the year 2010, additional stations have been installed within the framework of the Swiss Strong Motion Network (SSMNet) renewal (e.g., Clinton et al., 2011) and other projects in the region (Fig. 2a). Furthermore, real-time data exchange with neighboring seismic networks in southern Germany, France and Austria has been established at the same time to improve earthquake detection and location quality in the border regions (e.g., Diehl et al., 2021a, 2021b). Between the year 2012 and 2013, ten additional weak-motion stations have been installed in northern Switzerland and southern Germany on behalf of Nagra. This "third-generation" Nagra network aimed to achieve a magnitude of completeness (in our case defined as lowest local magnitude M_L that the network is able to record reliably and completely) of $M_C \leq 1.3$ in the three potential siting regions for deep geological nuclear waste repositories (Kraft et al., 2013). The network extension includes three short-period borehole stations installed at depths between 120 and 150 m below the surface and seven broad-band surface stations (Plenkers et al., 2015; Diehl et al., 2014). Since 2018, the Nagra network is locally densified with another six semi-permanent and two temporary surface stations, monitoring specific earthquake clusters and several exploration drilling campaigns in the region.

Fig. 2a documents the improvements in station density in the wider study area since about 2011. In addition to the network densification, the SED migrated to an improved seismic monitoring software in 2012 (Diehl et al., 2013), which, for instance, allows the usage of strong-motion stations in the automatic earthquake detection procedure and therefore also contributes to lower detection thresholds. In Fig. 2b the combined improvement is illustrated by the lowering of the detection thresholds by 0.5–1.0 M_L units and increasing slopes of cumulative sums of earthquakes as well as arrival-time picks since about 2013. M_C and its lateral variation in the study region are assessed with the probabilistic *PMC* method (Schorlemmer and Woessner, 2008), including several modifications described in Diehl et al. (2018). Our results in Fig. 2a document that the present-day network geometry (status as of September 2020) results in $M_C \leq 1.0$ for most parts of the study region. A similar *PMC* analysis for the network geometry as of December 2016 suggests an overall similar M_C in the region since the completion of the network extension in 2013 (Diehl et al., 2018). Estimates of M_C for periods prior to 2013 are documented in Nanjo et al. (2010) and Kraft et al. (2013). Apart from lower detection thresholds, the densified network also improves hypocenter location qualities as documented by Diehl et al. (2021b) and further discussed in the next section.

3.2. Earthquake catalogs and relocation procedures

The seismotectonic study of the HBG builds on the successive improvement of earthquake catalogs through several iterations of absolute and relative hypocenter relocations methods and merging procedures as summarized in Fig. S1. The final *MERGECAT* catalog contains hypocenter solutions of maximum possible hypocenter accuracy and precision for each event as described in detail in the following sections.

The proposed procedure starts from the SED earthquake bulletin (*BULCAT*, Fig. S1) covering the period 1975/01 to 2021/04 (46 years). The *BULCAT* catalog is the most complete one, associated locations, however, contain inconsistencies resulting from changes in location procedures (hypocenter location algorithms, velocity models, arrival-time picking, etc.) over time. Due to these changes, hypocenter uncertainties reported in such bulletins, if provided at all, are inconsistent as well and often underestimate the true location error (e.g., Diehl et al., 2021b; Lee et al., 2023). To overcome these limitations, the digital era of SED's instrumental catalog (starting 1984/01) was relocated by Diehl et al. (2021b), using an improved regional 3-D *Pg* and *Sg* velocity model in combination with the absolute nonlinear hypocenter location algorithm *NonLinLoc* (NLL, Lomax et al., 2000, Lomax et al., 2014) and a consistent selection of *Pg* and *Sg* phases. The resulting *RELOC-NLL* (Fig. S1) catalog provides consistent absolute locations with accuracies approaching sub-kilometer scales and reliable uncertainty estimates for well constrained hypocenters (Diehl et al., 2021b). For earthquakes in earlier periods with sparser station coverage and lower numbers of

available *Pg* and *Sg* phases this relocation procedure can fail or result in locations less constrained than the original *BULCAT* solution (Diehl et al., 2021b). Therefore, we merged the absolute locations of both catalogs into the *MERGECAT-ABS* catalog as summarized in Fig. S1. We prefer the *BULCAT* solutions only in cases for which the *RELOC-NLL* solution is missing (events before 1984 or failed due to insufficient number of *Pg/Sg* phases) or is less well constrained (e.g., azimuthal gap larger than the one of the *BULCAT* solution).

The *MERGECAT-ABS* catalog contains solutions of highest possible hypocenter accuracy (i.e., best absolute locations) and is used as initial catalog for improving the hypocenter precision through relative relocation. The main improvement in relative relocation methods is achieved by the additional use of differential times derived from waveform cross-correlations (e.g., Poupinet et al., 1984; Schaff et al., 2004). In our approach, we performed the waveform cross-correlation measurements in the time domain, followed by a sequence of quality checks to remove possible blunders as described in Diehl et al. (2017). We then applied the double-difference (DD) relocation algorithm *hypoDD* of Waldhauser and Ellsworth (2000) at different scales (Fig. S1). First, we performed DD relocations for five individual earthquake clusters located within the Hegau-Lake Constance region (Basadingen-Schlattingen, Bodanrück, Hilzingen 1995–1996, Hilzingen 2016–2020, Singen; see Fig. 3). These small-sized problems could be inverted using the Singular Value Decomposition (SVD) solver of *hypoDD*, and the regional 1-D *Pg* and *Sg* velocity models of Diehl et al. (2021b) were used for all relative relocations. The results of the individual clusters are discussed in detail in Section 4.2. The solutions of the five DD relocated clusters form the *RELOC-DDC* catalog (Fig. S1) and the quality of the individual DD inversions was assessed in detail. In a second step, we performed a DD relocation at a regional scale, solving for relative locations of all earthquakes included in Fig. 1 in one single DD inversion. The size of this problem requires the use of a damped least-square solver (Waldhauser and Ellsworth, 2000) and relative location can fail, for instance, for isolated or poorly constrained shallow seismicity. The results of the regional DD approach form the *RELOC-DDR* catalog.

Finally, we merged all three catalogs (*MERGECAT-ABS*, *RELOC-DDC*, *RELOC-DDR*) into the final *MERGECAT* catalog as summarized in Fig. S1. If existing, we preferred the *RELOC-DDC* solution over the *RELOC-DDR* solution. If no DD solution was available, we used the preferred absolute location of the *MERGECAT-ABS* catalog. Relative as well as absolute location uncertainties are reported for DD and NLL locations. Quantitative absolute location uncertainties of *BULCAT* solutions are unknown, however, a first-order, empirical quality rating can be derived from location parameters as proposed e.g., by Deichmann et al. (2000b). The *MERGECAT* catalog is available in digital form from a permanent data repository (see Data Availability Statement).

3.3. Focal mechanism catalog and stress-inversion analysis

In order to understand the kinematics of active faults of the HBG and their relation to the present-day stress regime in the northern foreland of the Central Alps, a catalog of high-quality, first-motion focal mechanisms (FM) has been compiled over the last decades. The FM catalog used in this study builds on the catalogs of Deichmann et al. (2000a) and Kastrup et al. (2004), complemented by mechanisms published in SED's annual earthquakes reports, which are available since 1996 (e.g., Baer et al., 1997; Deichmann et al., 2000b; Diehl et al., 2021a). In addition, it includes several unpublished new mechanisms from events occurring since 2019. The final FM catalog contains 51 solutions of events within the study region occurring between 1976 and 2021, with M_L ranging from 1.3 to 4.1 and focal depths ranging from 1 to 31 km (Fig. 3). The FM catalog is available in digital form from a permanent data repository (see Data Availability Statement). All mechanisms are derived from *P*-wave first-motion polarities. Different methods, however, have been used for the calculation of take-off angles and polarity fitting (e.g., Deichmann et al., 2000a; Kastrup et al., 2004). Since 2013, all take-off angles are consistently calculated within the 3-D *P* wave velocity model of Husen et al. (2003) using the NLL software and FM solutions are derived with the *HASH* algorithm (Hardebeck and Shearer, 2002) as described e.g., in Diehl et al. (2021a). The number of reliable moment tensor (MT) solutions derived from waveform inversion is sparse in the study region and therefore insignificant compared to the FM catalog. Since 2013, only two earthquakes of sufficient magnitude (usually $M_L \geq 3.5$) resulted in reliable MT solutions. One of them is presented in this study in Section 4.2. The MT inversion procedure used since 2013 is described in Diehl et al. (2021a).

A focal mechanism yields two possible focal planes (actual fault plane and auxiliary plane) and is therefore not sufficient to determine the geometry (i.e., strike and dip angle) and slip direction (i.e., rake angle) of the active rupture of an earthquake. The knowledge of the active fault plane, however, is crucial for the kinematic analysis of faults and to derive tectonic stress regimes from FM data (e.g., Michael, 1984; Kastrup et al., 2004). In case of small to moderate-size earthquakes, the active plane is usually determined from the geometry imaged by high-precision, relative relocations of fore- and aftershocks (e.g., Kastrup et al., 2004). To determine active planes in the study region, we therefore assessed our relative relocation catalogs in the surroundings of FM solutions and used additional information provided in the study of Deichmann et al. (2000a). In total, we reliably determined the active plane of 19 FM solutions from relative relocations (Fig. 3).

In order to determine the present-day principal stress directions in the wider Hegau-Lake Constance region, the FM catalog shown in Fig. 3 was used for a stress inversion. The inversion was performed with the *MSATSI* package of Martínez-Garzón et al. (2014), which is based on the stress-inversion algorithm of Hardebeck and Michael (2006). As proposed by Kastrup et al. (2004), we used both possible fault planes in the inversion in cases where the active plane of the FM was unknown. Where the active plane was determined from relative relocations, we used the active plane twice in the inversion, which corresponds to an effective doubling of the weight of uniquely determined slip data. To assess the uncertainty of the inversion, we performed a bootstrap resampling analysis of 2000 iterations. Due to the limited number of available FM solutions, we only performed 1-D stress inversions, i.e., we did not solve for 2-D or 3-D spatial variations within the inversion (see Martínez-Garzón et al., 2014). To resolve potential first-order spatial variations in the stress regime, we instead performed 1-D stress inversions separately for upper-crustal ($\leq$ 15 km depth) and lower-crustal ($>$ 15 km depth) seismicity within a wider region as well as specifically for earthquakes located within the HBG. The parameters resolved by the inversion are the orientations of the principal stress axes (S_1, S_2, S_3, with $S_1 > S_2 > S_3$) defined by their trend and plunge angles. In addition, we obtain the relative stress magnitude Φ, which is the ratio of the differences between the magnitudes of the three stress axes (e.g., Michael, 1984) defined as

$$\Phi = \frac{S_2 - S_3}{S_1 - S_3},$$

or, alternatively represented (e.g., Kastrup et al., 2004) by

$$R = 1 - \Phi = \frac{S_2 - S_1}{S_3 - S_1}.$$

Finally, we compare the orientations of the principal stress axes derived from the stress inversions with the orientation of seismically active faults of the graben.

4. Results

4.1. Relocated seismicity in the Hegau-Lake Constance region

Fig. 3 shows a tectonic summary map of the study region with the hypocenter locations of the *MERGECAT* catalog resulting from the relocation and merging procedure described in Fig. S1. In addition,

available focal mechanisms with active fault-plane solutions (if known) are displayed. We separated seismicity and associated focal mechanism into two different depth intervals ($\leq$ 15 km and $>$ 15 km) to identify possible first-order differences between upper and lower crust.

In the upper crust (Fig. 3a), the majority of seismicity occurs within the HBG, with its main activity limited by the Neuhausen Fault (NF) in the SW and the Bodanrück peninsula (BR) of Lake Constance in the NE. The main seismic activity of the graben appears to be limited by the Hegau Volcanics in the NW and an imaginary line Constance-Zurich in the SE. This imaginary line runs approximately parallel to the Alpine thrust front located about 40 km further to the south.

Another seismically active region in the upper crust locates in front of the Subalpine Molasse (Fig. 3a) within the Alpine foreland triangle zone, immediately north of the Alpine thrust front (e.g., Pfiffner, 1986; Heuberger et al., 2016). It coincides with the southernmost segments of the N-S to NE-SW striking St. Gallen Fault Zone (SFZ; Heuberger et al., 2016). In 2013, a seismic sequence (FM solutions U10–11 in Fig. 3a) indicating sinistral strike slip was induced by reservoir stimulation and mud-control measures in a deep geothermal well. This seismicity indicates that the southern part of the SFZ is critically stressed (Diehl et al., 2017). Further to the north, a possible prolongation of the SFZ has been found to offset Quaternary sediments within Lake Constance, providing further geological evidence for its present-day activity (Fabbri et al., 2021). Seismicity north of Arbon, beneath Lake Constance (FM solution U1 in Fig. 3a) could possibly also be related to the SFZ.

A cluster of lower-crustal seismicity in the center of the HBG (e.g., FM solutions L1, L9, L14, L19 in Fig. 3b) suggests that seismicity below the graben structure might reach depths of 20 km and more. This cluster also includes the M_L 4.1 Steckborn earthquake of 1986 (FM solution L1 in Fig. 3b, focal depth about 17 km), the strongest instrumentally

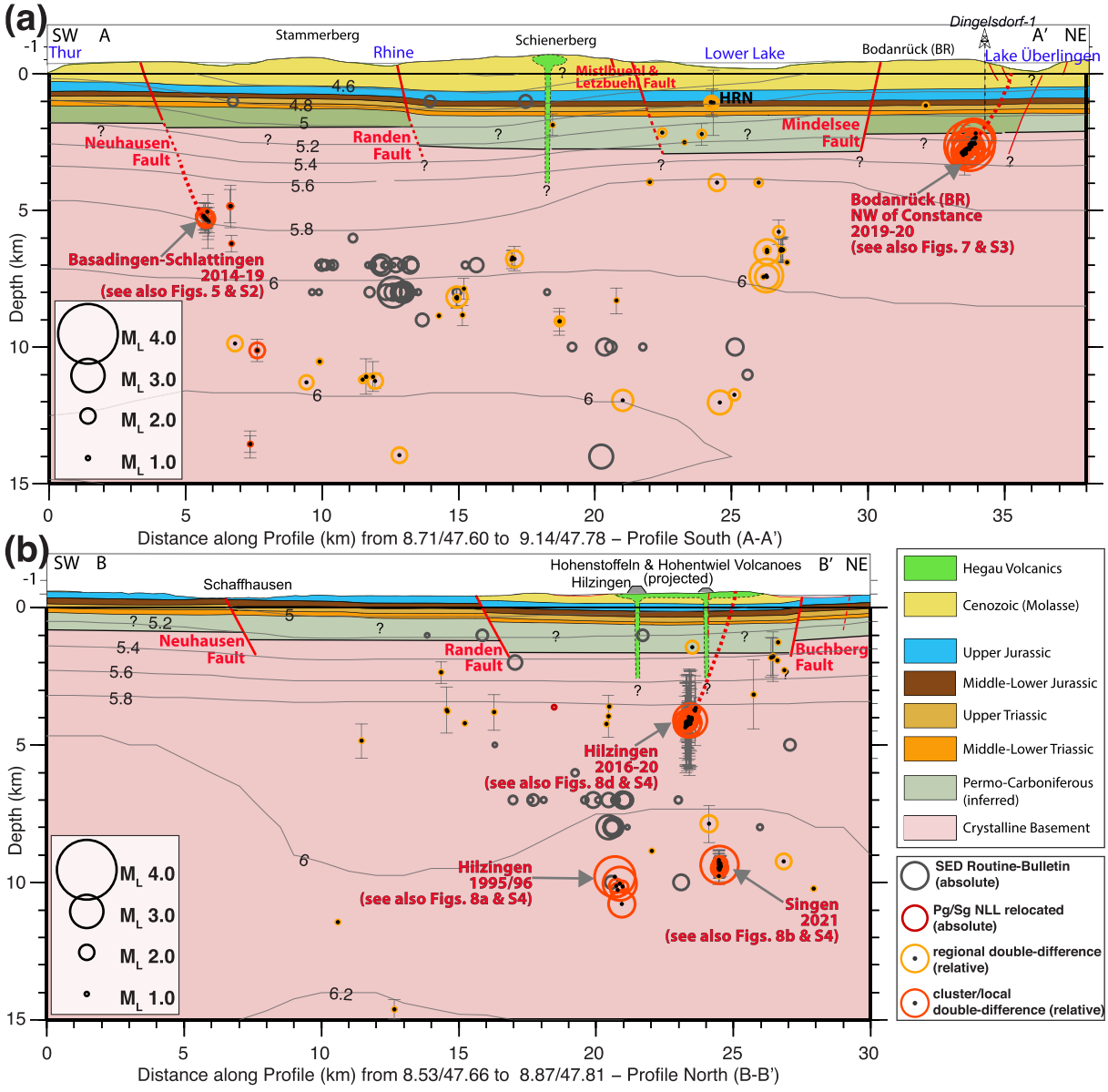

Fig. 4. Two vertical, upper-crustal cross-sections of the Hegau-Bodensee Graben combining geological and geophysical information. See Fig. 3b for location of profiles. The geological cross-sections were constructed on the basis of existing geological models provided by Nagra (2008) and Allenbach et al. (2017). Contour lines indicate *P*-wave velocities (km/s) derived by the local earthquake tomography model of Diehl et al. (2021b). Displayed seismicity is taken from the *MERGECAT* catalog (Fig. S1), including absolutely and relatively relocated hypocenters as explained in the legend. Only seismicity within the corresponding gray boxes shown in Fig. 3b is projected to the profiles. Error bars indicate the 1σ vertical uncertainty of absolute hypocenter locations derived by the NLL location algorithm. No vertical uncertainties are shown for bulletin locations since errors are unknown or inconsistently measured.

recorded earthquake in the study region (e.g., Deichmann et al., 2000a). The focal plane solution of this earthquake indicates a transtensional mechanism. Additional lower-crustal seismicity appears to be concentrated within a corridor extending toward the SE of the graben and which terminates north of the triangle zone (Fig. 3b).

Since 1995, several remarkable earthquake sequences occurred in the graben, which provide important constraints into geometry and kinematics of associated faults. We analyzed five of these sequences (Basadingen-Schlattingen, Bodanrück Peninsula, and three sequences in the Hegau region near the towns of Singen and Hilzingen) in detail and corresponding results are provided in the following sections. These relocated sequences are also displayed in the two larger-scale cross-sections of the graben in Fig. 4. Additional maps and cross-sections presented in Figs. S2-S4 document the extrapolation toward the surface of the relocated sequences as well as possible connections with known faults and topography in more detail.

4.2. Analysis of earthquake sequences in the Hegau-Bodensee Graben

4.2.1. Basadingen-Schlattingen earthquake sequence and its link to the Neuhausen Fault

Between 2014 and 2016 a microseismic earthquake sequence occurred close to the town of Basadingen-Schlattingen, about 10 km SE of the city of Schaffhausen (Fig. 3a). The epicenter of the sequence locates about 3–4 km NE of the surface outcrop of the Neuhausen Fault (NF in Figs. 3a, 4a and S2). A FM solution could be derived for the largest event of the sequence (M_L 2.2, solution U14 in Fig. 3a). Its normal-fault character in combination with the fault geometry imaged by earlier relative relocation efforts, already suggested a possible link of the seismic sequence to the Neuhausen Fault (Diehl et al., 2018). In 2019, three additional seismic stations were installed along the Neuhausen Fault, which recorded another M_L 2.1 earthquake in September 2019. The FM solution of this event (solution U29 in Fig. 3a) is very well constrained and shown in Fig. 5 together with the FM of the 2015 event and the hypocenters derived by the relative relocations of the cluster (*RELOC-DDC* catalog, Fig. S1). The results of the relative locations in the cross-section of Fig. 5b are consistent with the variation of the two focal mechanisms, indicating a down-dip decrease in fault dip toward NE. This decrease suggests a listric shape of the NE dipping normal fault. According to the geological profile, the focal depth of 5–6 km corresponds to a fault within the crystalline basement, consistent with tomographic *P*-wave velocities (v_P) of about 5.8 km/s in the source region of this cluster (Fig. 4a). The dip indicated by focal mechanisms and their relative locations allow for a connection of this seismic cluster with the Neuhausen Fault as documented by Fig. S2. This interpretation suggests that the Neuhausen Fault has a listric geometry and extends at least 3–4 km into the crystalline basement.

4.2.2. The Bodanrück earthquake sequence NW of Constance

Between July 2019 and May 2020, a remarkable earthquake sequence occurred on the Bodanrück peninsula of Lake Constance, located about 8 km NW of the city of Constance (BR in Figs. 3 and 4a). The strongest event ($M_L = 3.7$, $M_W = 3.3$; Fig. 6a) was associated with a first phase of activity between July 29 and 31, 2019. This event was preceded by an M_L 2.8 foreshock occurring 11 min earlier (Fig. 6b) and was followed by a series of aftershocks with magnitudes up to M_L 3.2 (Figs. 6c-6e). A second phase of intense activity started on August 29 and lasted till mid-September 2019, including an M_L 3.4 and M_L 3.0 event (Figs. 6f-6g).

In total, seven high-quality FM solutions were calculated for this sequence (Fig. 6), all of them indicating normal-fault mechanisms with a minor strike-slip component. A moment-tensor solution was derived for the M_L 3.7 event (Fig. 6a, bottom), which is quite similar to the corresponding FM solution. Only the FM of the M_L 3.1 event of July 31 (Fig. 6e) shows larger discrepancies in comparison with the other solutions in Fig. 6. The *P*-wave polarity at the closest station WALHA is

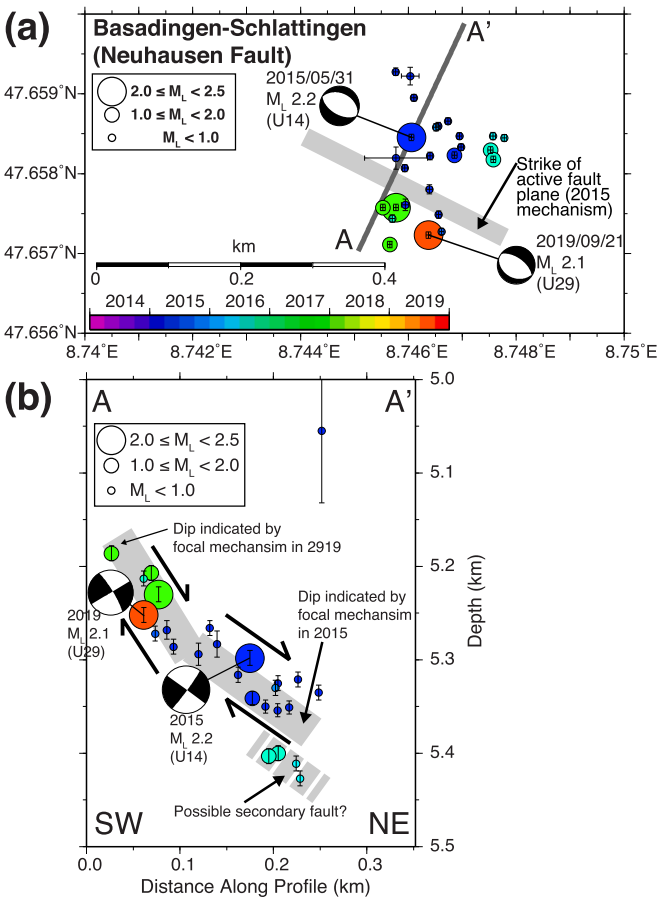

Fig. 5. Focal mechanisms (FM) and relative relocations of the Basadingen-Schlattingen microearthquake sequence (see Figs. 3a and S2 for location), likely occurring along a deep, listric prolongation of the Neuhausen Fault within the crystalline basement. Colors indicate origin time of earthquakes; error bars correspond to relative-location uncertainties as derived by the SVD inversion. (a) Map view. (b) Vertical cross-section along a profile oriented perpendicular to the strike of the focal-plane solution of the M_L 2.2 event of 2015. Solid gray lines in (b) indicate a first-order fault-geometry model, considering the dip of the two FMs, the spread of the relative relocations and associated vertical location uncertainties. Potential extrapolations of the fault to the surface are shown in Fig. S2. FMs are shown as lower-hemisphere stereographic projection in map view and projected ("side view") to the depth profile in cross-section. FM labels U14 and U29 correspond to the labels used in Fig. 3a.

upward for this mechanism, while downward for all other mechanisms (Fig. 6), indicating potential variations in the fault dip.

In agreement with the majority of focal mechanisms, the relative relocations of the sequence in Fig. 7 image a normal fault, which dips about 40° toward the SW. The remarkably shallow dip of this normal fault suggests the reactivation of a Late Paleozoic normal fault (Madritsch et al., 2018 with references therein). The only deviation from this trend is represented by the above-mentioned M_L 3.1 event of July 31, which suggests a significantly steeper dip of about 70° (Fig. 7b) and might indicate the existence of second-order fault structures. The shallow depth of 2–3 km of the sequence is well constrained by observations at the seismic station WALHA, located at a distance of 2 km from the epicenter. The comparison with the geological model in Fig. 4a suggests a source within the top part of the crystalline basement. Due to general uncertainties in pre-Mesozoic basement structures in this part of the northern Alpine foreland (Diebold et al., 1991; Madritsch et al., 2018) and lower tomographic v_P values of about 5.4–5.6 km/s in the source region (Fig. 4a), we cannot entirely rule out a location within Permocarboniferous sedimentary units. The extrapolated surface

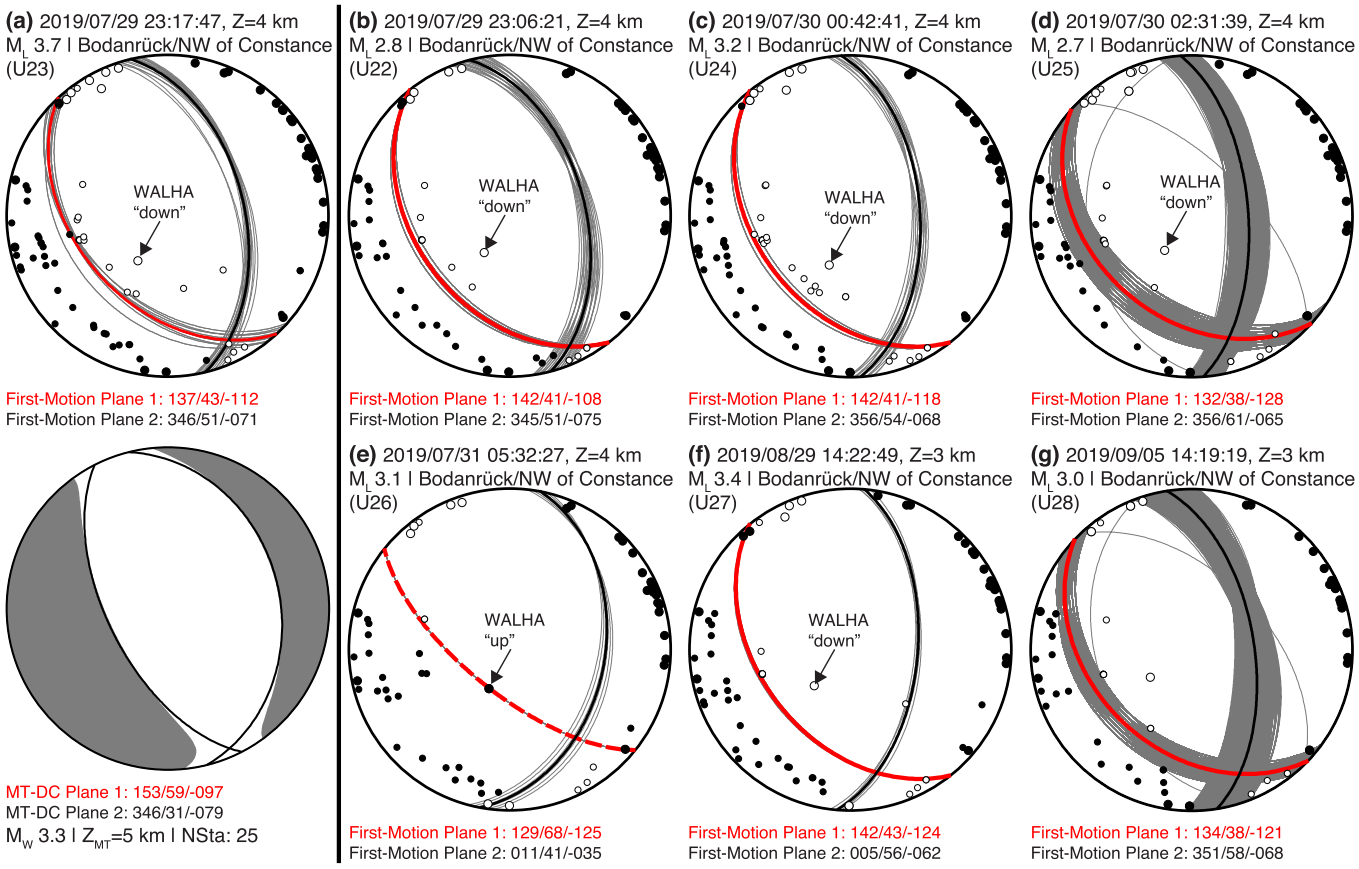

Fig. 6. Focal mechanisms of the Bodanrück sequence NW of Constance in 2019. (a) Fault-plane solution (lower hemisphere, equal-area projection) of the largest event of the sequence based on first-motion (FM) polarities (top) and corresponding full-waveform moment tensor (MT) solution (bottom). (b)-(g) FM solutions of additional six events of the same sequence. Solid circles correspond to compressive first motion (up); empty circles correspond to dilatational first motion (down). Gray lines show sets of acceptable solutions derived by the *HASH* algorithm; black, bold lines indicate the (preferred) average focal mechanism of all accepted solutions; red, bold lines mark the active plane as determined from high-precision relative relocations. Information on origin time, bulletin focal depth in km below mean sea level (Z) and the two focal planes (defined by strike/dip/rake angles as defined by Aki and Richards, 2002) is provided above and below each mechanism. The strike/dip/rake of the double-couple part of the MT (MT-DC) as well as the associated moment magnitude (M_W) are provided below the MT solution. FM labels U22–28 correspond to the labels used in Fig. 3a. (For interpretation of the references to colour in this figure legend, the reader is referred to the web version of this article.)

outcrop of the imaged fault locates between the NE coast of the Bodanrück peninsula and the Überlinger branch of Lake Constance (Figs. 3, 4a and S3). Absolute horizontal and vertical location uncertainties are <1 km and therefore it is not possible to associate the sequence with the Mindelsee Fault (MF in Figs. 3 and S3) or any other previously mapped SW-dipping fault in Figs. 3, 4a and S3.

4.2.3. Earthquake sequences in the Hegau region near Hilzingen and Singen

The Hegau region hosted three noteworthy earthquake sequences since 1995 and Fig. 8 summarizes the corresponding relative relocations and available FM solutions. Between 1995 and 96, a small sequence of earthquakes occurred SW of the town of Hilzingen, located about 6 km west of Singen (Figs. 3 and S4). A first analysis of this sequence was provided by Deichmann et al. (2000a). Instrumentation at that time was much sparser, resulting in significantly fewer events and larger relative-location uncertainties (Fig. 8a). In agreement with relative relocations computed by Deichmann et al. (2000a) and their conclusions, we interpret the WNW-ESE striking dextral solution as the active fault plane (Fig. 8a). The sub-vertical fault suggested by the fault-plane solution locates at a depth of about 10 km and therefore certainly within the crystalline basement (Fig. 4b).

The sequence which occurred north of Hilzingen between 2016 and 20 (Fig. 8c and d) has been previously described by Stange et al. (2017) and Diehl et al. (2018). The main seismic activity occurred in November 2016 and FM and relative relocations image a dextral transtensional fault, dipping at an angle of about 60° toward SW. Seismicity occurring in January and March 2020 locates up-dip of the main structure (active during 2016–2017; Fig. 8d), indicating a possible steepening of the fault in up-dip direction similar to the listric geometry proposed for the Neuhausen Fault in Fig. 5b. For a subset of events, absolute depths of 4.0–4.5 km were additionally constrained by an aftershock station installed about 2 km from the epicenter by the Landeserdbebendienst Baden-Württemberg in Freiburg, Germany. The geological model and tomographic v_P values of about 5.8 km/s in the source region suggest that the imaged fault is likely located within the crystalline basement (Fig. 4b). Similar to the Bodanrück sequence (Section 4.2.2), we cannot associate this SW-dipping fault with any previously mapped fault in the region (Figs. 4b). However, considering the remaining uncertainties in location and fault dip as documented by Fig. S4, a link to the SW-dipping Hegau or Buchberg Faults cannot be completely ruled out.

In February 2021, another earthquake sequence in the Hegau region occurred near the city of Singen, located about 4 km SE of the 2016 Hilzingen cluster (Figs. 8b and S4). The FM solution of an M_L 3.2 earthquake combined with relative relocations image a dextral, sub-vertical fault, located at a depth of about 10 km (Figs. 3 and 8b). As was the case for the sequence of 1995–96, this fault is certainly located in the crystalline basement and likely not related to any previously mapped structure (Fig. 4b). However, a connection to the Hegau Faults

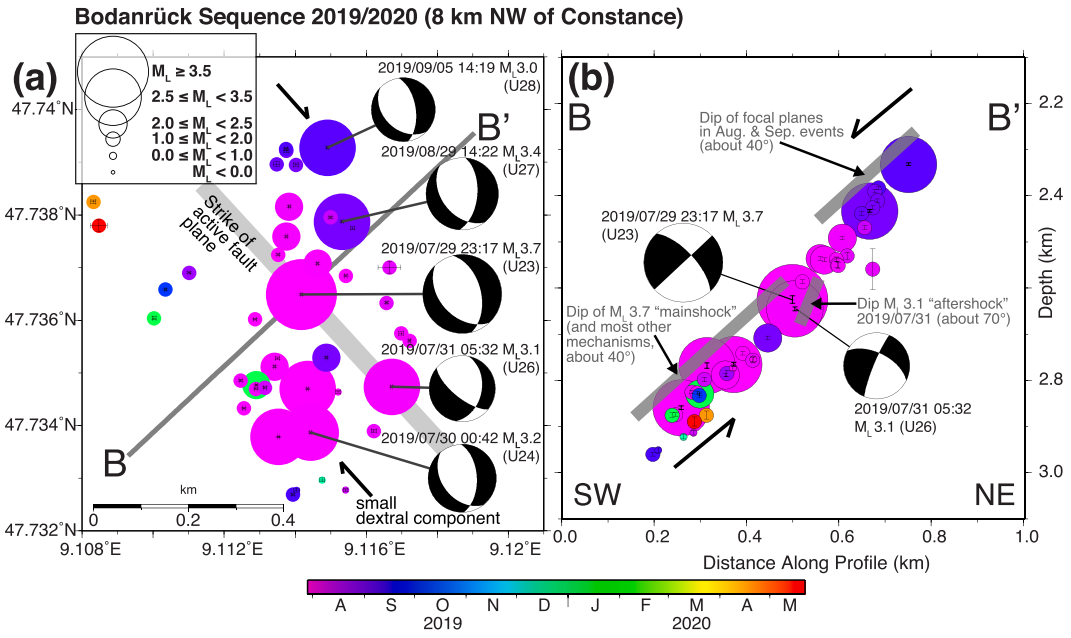

Fig. 7. Relative relocations and selected focal mechanisms (FM) of the Bodanrück sequence NW of Constance (see Figs. 3a and S3 for location). Colors indicate origin time of earthquakes; error bars correspond to relative-location uncertainties as derived by the SVD inversion. (a) Map view. (b) Vertical cross-section along a profile oriented perpendicular to the strike of the focal plane solution of the M_L 3.7 event of July 2019. Potential extrapolations of the fault to the surface are shown in Fig. S3. Focal mechanisms are shown as lower-hemisphere stereographic projection in map view and projected ("side view") to the depth profile in cross-section. FM labels U23–24 and U26–28 correspond to the labels used in Fig. 3a.

cannot be completely ruled out (Fig. S4a).

4.3. Stress inversion and fault kinematics

As can be seen in Fig. 3, the FM solutions in the Hegau-Lake Constance region are dominated by normal and strike-slip faulting mechanisms. In order to derive the present-day orientations of the principal stress axes and possible lateral or vertical variations, we performed a stress inversion following the procedure described in section 3.3. Fig. 9 shows the results derived for three different subsets of FMs. In Fig. 9a, we used 21 upper-crustal (depth $\leq$ 15 km) FMs located within the graben (FMs within box outlined by gray dashed line in Fig. 3a) in the inversion. For 15 FM solutions the active planes were all roughly striking NW-SE as inferred from relative relocations ($N_{KnownFault}$ in Fig. 9). The best fitting principal axes correspond to a normal-fault regime with an almost vertical S_1 axis and horizontal S_3 axis. The horizontal orientation and the WSW-ENE azimuth of the S_3 axis is well constrained. The S_1 and S_2 axes resulting from the bootstrap resampling, however, form an NNW-SSE oriented band, indicating that the plunge of both axes is not well resolved and magnitudes of S_1 and S_2 are similar. This is also reflected by the relatively high Φ value of 0.73. The interchangeability of S_1 and S_2 axes is therefore symptomatic for a transtensional stress regime of the graben with a dominating normal-fault component.

A similar result is obtained for all 32 upper-crustal FMs in the wider study area (all FMs included in Fig. 3a), showing an even more pronounced interchangeability of S_1 and S_2 axes (Fig. 9b). The transtensional stress regime of the graben is therefore largely consistent with the regional one within the upper crust of the northern Central-Alps foreland in NE Switzerland. Finally, we also performed an inversion of 19 FMs located in the lower crust (all FMs included in Fig. 3b) shown in Fig. 9c. In comparison to Fig. 9b, we observe a minor, about 10° counterclockwise rotation of the S_3 axis in the lower crust. In contrast to the upper crust, the best-fitting solution shows an almost vertical S_2 and a horizontal S_1 axis, suggesting a strike-slip regime in the lower crust. The same interchangeability of S_1 and S_2 axes as observed for the upper crust, however, indicates a similarly orientated transtensional stress regime (with a dominating strike-slip component) in the lower crust in agreement with previous studies (e.g., Kastrup et al., 2004; Singer et al., 2014).

In Fig. 9d, we compare the strike of faults associated with the HBG (estimated from map as well as from individual FM solutions with known active planes) with the trend of the S_1 and S_3 axes. The angle Θ between fault strike and S_1 is in the order of 20° to 30°, which suggests that faults of the HBG are favorably to optimally orientated to be reactivated (in dextral sense) in the present-day stress regime (e.g., Sibson, 1990). Fig. 9e displays fault dip as a function of rake angle (slip direction) for upper-crustal FMs in the graben (same selection as for Fig. 9a). Both possible FM planes are plotted for solutions with unknown active plane. Consistent with the transtensional stress regime, the majority of rake angles are negative. In addition, all known fault planes show dextral components, with the exception of one almost pure normal-fault mechanism, which plots at the boundary between dextral and sinistral. The fault dip of know planes varies between about 36° to 88°. Especially the dip of about 40° observed for the Bodanrück sequence is rather low-angle and appears less favorably oriented for the predominantly normal-faulting mechanisms.

5. Discussion

5.1. Imaging of seismically active faults of the Hegau-Bodensee Graben

In general, seismic activity in the HBG over the past 46 years is low. Nevertheless, owing to the significant improvement in seismic instrumentation since about 2011, several seismogenic faults could be identified. Furthermore, the new data as well as advanced seismological methods constrain the lithologies hosting these seismogenic faults and their geometries with unprecedent resolution. Our results suggest that the majority of seismogenic fault segments associated with the graben locate within the crystalline basement (Fig. 4). These basement-rooted faults support the interpretation of the graben's crustal-scale nature (Egli et al., 2017). In its southeastern part, we associate the cluster near Basadingen-Schlattingen located at depths of 5–6 km with the root of the

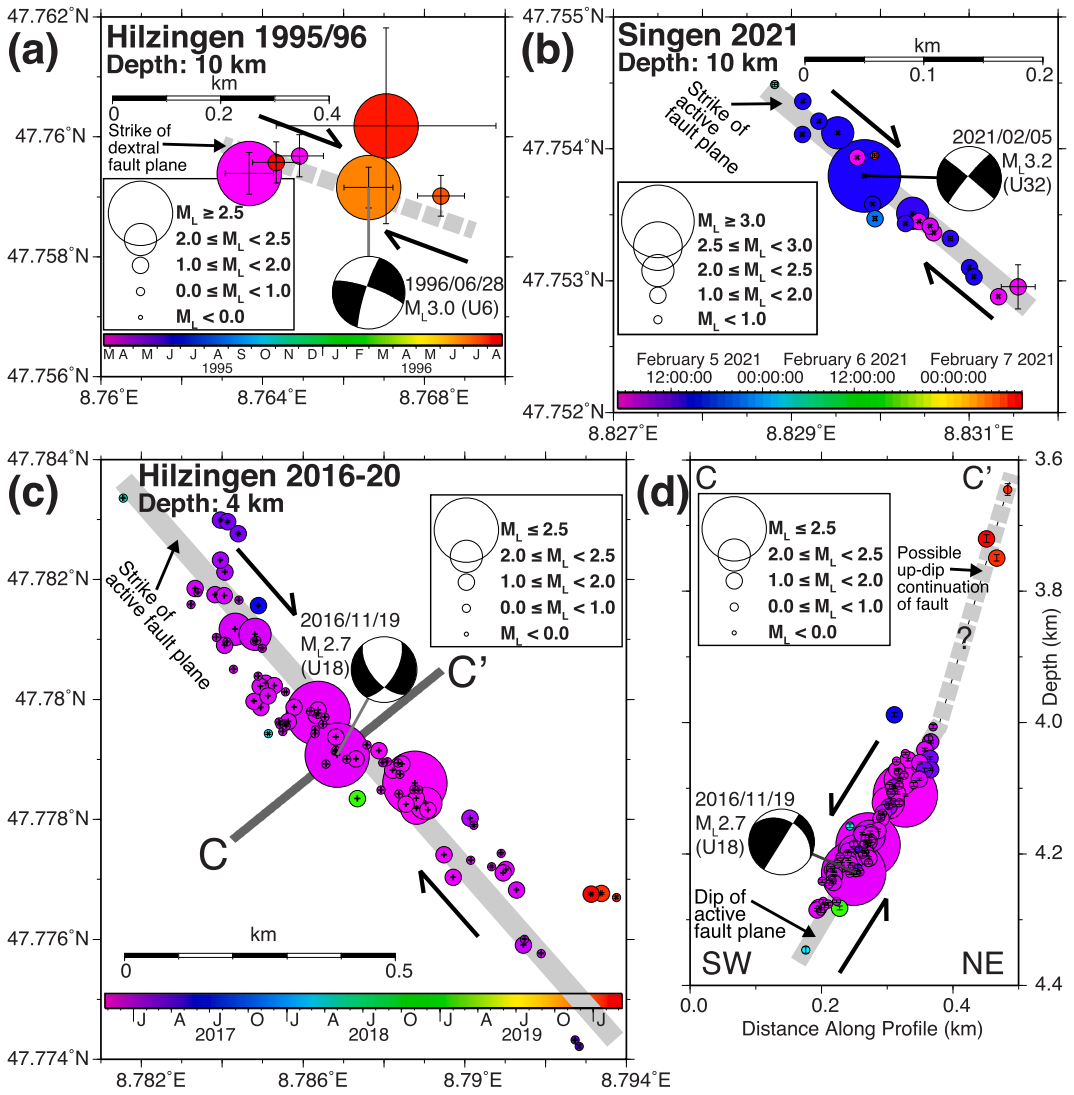

Fig. 8. Relative relocations of three sequences in the Hegau region near the towns of Hilzingen and Singen (see Fig. 3a and S4 for location). Colors indicate origin time of earthquakes; error bars correspond to relative-location uncertainties as derived by the SVD inversion. (a) Map view of the 1995/96 Hilzingen sequence. (b) Map view of the Singen sequence of 2021. (c) Map view of the 2016 Hilzingen sequence. (d) Vertical cross-section of the 2016 Hilzingen sequence along a profile oriented perpendicular to the strike of the dextral focal plane solution of the M_L 2.7 event of November 2016. Potential extrapolations of the fault to the surface are shown in Fig. S4. Focal mechanisms (FM) are shown as lower-hemisphere stereographic projection in map view and projected ("side view") to the depth profile in cross-section. FM labels U6, U18 and U32 correspond to the labels used in Fig. 3a.

NE-dipping Neuhausen Fault within the crystalline basement. This fault seems to limit the graben toward the SW (Fig. 4a). The SW-dipping fault imaged by the Bodanrück sequence in about 2–3 km depth, on the other hand, represents a possible conjugate boundary fault on the opposite side of the graben, likely located within the topmost crystalline basement (Fig. 4a). As documented by Figs. 3 and 4a, seismicity within these boundary faults can be tracked to depths of at least 20 km (e.g., FM solutions L9, L14, L18 in Fig. 3b), suggesting that almost the entire crust deforms in a brittle regime in this central part of the graben.

In the northern part of the graben, seismicity is concentrated in the region of the Hegau Volcanic edifices, reaching depths of about 10 km (Figs. 3 and 4b). The Hilzingen sequence of 2016 images as SW-dipping fault in about 3.5–4.5 km depth within the topmost crystalline basement (Fig. 4b), similar to the Bodanrück structure. The two other sequences (Hilzingen 1995 and Singen 2021) locate deeper, at about 10 km, and represent sub-vertical strike-slip faults. Although the proximity of the sequences to the Hegau Volcanic edifices is conspicuous (Figs. 3a, 4b and S4), a possible connection between the present-day seismicity and the Miocene volcanic activity remains speculative.

Only few well-constrained hypocenters locate within Cenozoic or Mesozoic sediments of the graben (Figs. 3a and 4). One potential cluster locates below the Lower branch of Lake Constance near the town of Horn (FM solution U21 in Fig. 3a; HRN in Fig. 4a). Waveforms of these events show pronounced surface-wave coda, characteristic for shallow sources within the sedimentary cover (e.g., Lanza et al., 2022). Absolute depth uncertainties of these locations, however, are too large to precisely determine the lithology hosting the source.

The general lack of seismicity within sedimentary units hinders to establish reliable links between seismogenic structures in the basement and geologically mapped or geophysically imaged faults in the sedimentary cover. Only the Basadingen-Schlattingen structure can be associated with large confidence to the Neuhausen Fault, which is well imaged by seismic reflection surveys (Birkhäuser et al., 2001; Roche et al., 2020) and further to the NW also recognized in outcrops of Mesozoic limestone (Hofmann, 1981). All other sequences discussed in Section 4.2 cannot be reliably linked to previously mapped faults. In turn, major faults such as the Randen Fault (e.g., Egli et al., 2017) show little evidence for seismic activity over the past 46 years (Fig. 4). Two

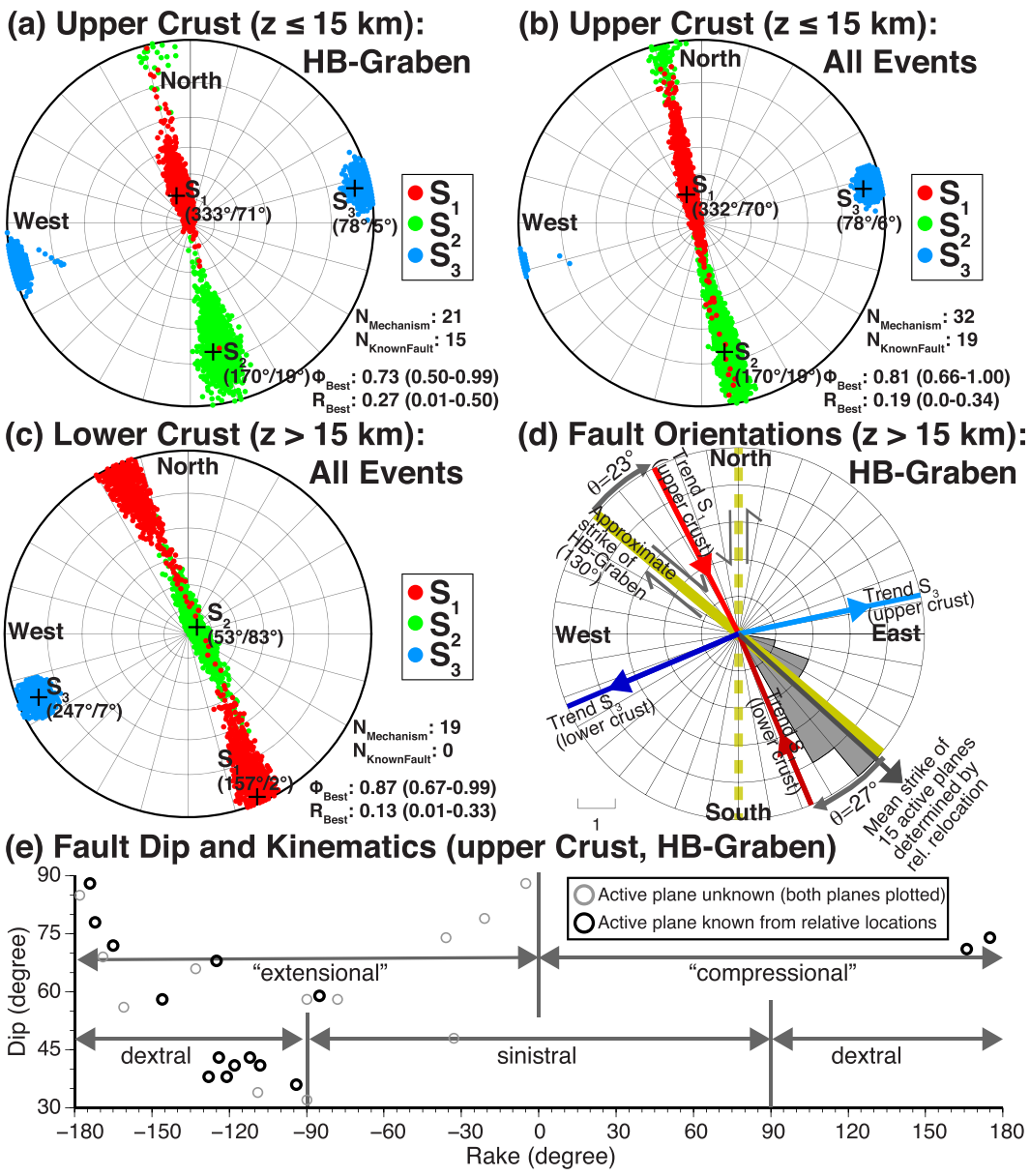

Fig. 9. Results of the stress inversion and the analysis of fault geometries and kinematics derived from first-motion focal mechanisms (FM) in the Hegau-Lake Constance region. (a) Stereonet projections of principal stress axes S_1-S_3 ($S_1 > S_2 > S_3$) derived from the inversion of upper-crustal FM solutions in the Hegau-Bodensee (HB) Graben (FMs included in dashed, gray box in Fig. 3a). Colored dots represent inversion results of 2000 bootstrap subsamples; crosses indicate the best solution with the axis's azimuth and plunge indicated in brackets. R and Φ values reflect the relative stress magnitude (see text for details). (b) Corresponding results derived from the inversion of all upper-crustal FMs in the region (all FMs shown in Fig. 3a). (c) Corresponding results derived from inversion of all lower-crustal FMs in the region (all FMs shown in Fig. 3b). (d) Strike of graben faults (yellow line: average strike from map; gray rose-diagram bars: FM strike as indicated by relative relocations of sequences; gray arrow: corresponding mean FM strike) in comparison to trend of S_1 and S_3. The angle between fault strike and S_1 on the order of 20°-30° degree suggests that the graben faults are favorable to optimally oriented to be reactivated in dextral strike-slip sense in the present-day stress field. Dashed yellow line indicates optimally oriented conjugated (sinistral) fault, potentially reactivated by the same stress regime. (e) Fault dip as function of rake angle (slip direction) for upper-crustal FMs in the graben (same FMs as in (a)). (For interpretation of the references to colour in this figure legend, the reader is referred to the web version of this article.)

hypocenters located at depths of 1–2 km near the Randen Fault in Fig. 4b are SED-bulletin locations, which we considered as unreliable solutions with significant location uncertainties.

Looking beyond the existing seismic data and outcrops of Mesozoic limestone, tracing faults to the surface is very difficult in the area of investigation due to the fact that robust evidences for outcropping faults (e.g., fault scarps) are very rare and fault maps in the region are mainly based on rubble stone field mapping (e.g., Ibele, 2015). Considering remaining uncertainties in the absolute hypocenter locations (on the order of few hundred meters for epicenters and up to 1 km for focal depths for well-constrained locations; see Diehl et al., 2017, 2021b; Lee et al., 2023) as well as in fault dip (and its up-dip extrapolation), no obvious geomorphological features can be related with confidence to one of the seismogenic fault planes imaged by microseismicity as documented by Figs. S2-S4. On the other hand, the overall strong imprint of fluvial and glacial surface processes in the region with rates exceeding tectonic processes may have masked previously existing surface fault scarps. More detailed analyses of high-resolution topographic data (such as Lidar images) and near surface sediments necessary for a thorough appraisal in this regard was beyond the scope of this

study. With the currently available data, we can thus not conclusively answer the question whether these seismogenic faults are related to blind faults or if they reach the surface (weathered Molasse or even the Quaternary sediments).

5.2. Present-day stress field and orientation of seismically active faults

As summarized in Fig. 9e, the majority of the FM solutions within the HBG correspond to strike-slip, normal-fault, or oblique mechanisms, suggesting a dextral transtensional deformation regime with a strong extensional component. This regime is consistent with the orientation of the principal stress axes (S_1, S_2, S_3) and relative stress magnitudes (Φ, R) derived from the inversion of FM solutions (Fig. 9). Our stress inversion results are in good agreement with previous regional studies of Kastrup et al. (2004), which find a similar interchangeability between S_1 and S_2 along an NNW-SSE (trend of S_1 between 165 and 169°) striking band for FM solutions in northeastern Switzerland ("region F5" in Kastrup et al., 2004). Reinecker et al. (2010) estimate a trend of 150° ± 24° for the maximum horizontal stress orientation (S_H), using various data types included in the *World Stress Map* database within the greater northern foreland of the Central Alps. Our results are also consistent with results derived by Egli et al. (2017) from the kinematic analysis of outcrop-scale fractures and slip vector modeling, suggesting extension and strike-slip faulting associated with graben structures during Miocene to recent times, as well as regional paleostress reconstructions (Madritsch, 2015; Ring and Gerdes, 2016).

The general orientation of the stress axes within the graben seems to follow the regional trend observed for the northeastern foreland of the Central Alps. The shallow part of the graben, however, seems to be characterized by a stronger tensional component in comparison with other regions in the northern foreland. In addition, we observe no significant change with depth as shown in Fig. 9, suggesting that the tectonic stress regime remains almost uniform throughout the entire crust (except for the uppermost 1–2 km, with reduced overburden and laterally variable overburden). Due to these similarities between lower- and upper-crustal stress regimes, possible driving forces of the present-day reactivation of the graben could be related to large-scale geodynamic processes such as slab-rollback dynamics proposed to explain the peculiar occurrence of lower-crustal seismicity in the northern foreland of the Central Alps (Singer et al., 2014; Kissling and Schlunegger, 2018).

Irrespective of the geodynamic processes causing the present-day transtensional regime in the northern foreland, it appears that NW-SE striking structures are preferably reactivated. As shown in Fig. 9d, the angle between the strike of the graben faults and the trend of the S_1 axis derived in our study is on the order of 20°-30°. Assuming friction coefficients μ_s between 0.6 and 0.85, the pre-existing graben faults are favorably to optimally oriented to be reactivated in a dextral strike-slip sense (e.g., Sibson, 1990).

Under the same stress field, N-S striking foreland faults forming conjugates to the previously discussed NW-SE striking ones, would be optimally oriented to be reactivated in sinistral strike-slip sense (dashed yellow line in Fig. 9d). Our data do not show any reactivation of such conjugated N-S striking fault systems within the region of the graben. However, vague evidence for reactivation of such an NNW-SSE striking fault was reported from hydraulic stimulations tests performed during a small-scale geothermal project near Basadingen-Schlattingen (Kraft et al., 2016). Toward the SE part of the study region, the situation appears to be different. A prominent example is the N-S to NNE-SSW striking St. Gallen Fault (SFZ in Fig. 3), which was reactivated in sinistral strike-slip sense during a geothermal project in 2013 (Diehl et al., 2017). Its presumed northward prolongation offsets Quaternary sediments in Lake Constance (Fabbri et al., 2021). The Albstadt shear zone (e.g., Mader et al., 2021) represents another N-S striking seismogenic zone north of the HBG.

While the kinematic concept of seismogenic faulting along NW-SE and N-S striking faults is consistent with the present-day stress field, our study has also shown that seismicity can be found along less favorably oriented structures. Examples are the normal-fault events along a low-angle fault (dip ~40°, see Figs. 7b and 9e) associated with the Bodanrück sequence NW of Constance. Reactivation of such unfavorably oriented faults may indicate fluid pressures elevated well above hydrostatic values (e.g., Sibson, 1990) or more complex kinematic interactions between seismogenic structures in the upper crust.

5.3. Comparison with historical seismicity

Our analysis of instrumentally recorded seismicity over the past 46 years suggests that the NW-SE striking bounding faults of the HBG (1) root in the crystalline basement (maximum depth up to 20 km), (2) are seismically active and (3) are favorably to optimally oriented to be reactivated in a dextral, transtensional sense in the present-day stress field. Seismic activity (i.e., number of earthquakes) and magnitudes over the 46-year period, however, are comparably small (maximum M_L = 4.1).

In order to assess the long-term seismogenic potential of faults at the southwestern edge of the graben (Neuhausen and Randen Faults), we compare the instrumental catalog with the historical seismicity reported in the earthquake catalog of Switzerland (ECOS-09; Fäh et al., 2011). Fig. 10a shows the historical earthquakes within the study region of either $M_W \geq 4.0$ or EMS-98 macroseismic intensities ≥ V. The maximum magnitude reported in the ECOS-09 catalog along the southwestern edge of the graben (area outlined by box in Fig. 10a) over the past 600 years is $M_W = 4.7$ and the total sum of the seismic moment M_0 released in the same period corresponds to an $M_W = 5$ earthquake (Fig. 10b). The occurrence of an $M_W > 6.0$ earthquake within the graben in the past 1000 years appears rather unlikely, since its macroseismic impact would have been likely documented in historical sources over a large region and no indication for such an event is included in the ECOS-09 catalog. On the other hand, the completeness of the historical ECOS-09 catalog in this region is virtually undefined before the year 1400 and reported to be intensity VI-VII for the period 1400–1800 (Fäh et al., 2011). Therefore, we cannot completely rule out the occurrence of moderate-sized earthquakes in this region missing in the ECOS-09 catalog before 1800.

The ECOS-09 catalog reports twelve $M_W = 3.9$ earthquakes, which occurred between 1542 and 1817 in the region of Schaffhausen (Fig. 10a and b). Although uncertainties of macroseismic locations are on the order of several kilometers (Fäh et al., 2011), the proximity to the Neuhausen as well as Randen Faults suggests a connection to either of these faults. Similarly, the $M_W = 4.7$ Stein am Rhein earthquake of 1573 as well as the $M_W = 4.2$ Rheinau earthquake of 1750 (Fig. 10a and b) might be related to bounding faults of the graben. Alternatively, the latter might also be related to a vigorous earthquake sequence close to the town of Eglisau, which includes >60 events with M_W up to 3.9 reported since the seventeenth century (Fig. 10a). The largest magnitude in the wider region is associated with the $M_W = 5.1$ earthquake near Amriswil, south of Lake Constance in 1771, which might be related to the northern segment of the St. Gallen Fault (Fig. 10a).

The analysis of the historical seismicity over the past 600 years therefore indicates that faults associated with the graben have the potential to generate magnitudes up to $M_W = 5$ in the Hegau-Lake Constance region. According to the empirical relationships of Wells and Coppersmith (1994), potential fault width of the basement-rooted faults on the order of 3–5 km as suggested by Figs. 4 and S2-S4 (assuming the faults reach the surface), on the other hand, would be sufficient for even larger magnitudes. It should be noted that the moment release during the 46-year period of instrumental recording is comparatively low (Fig. 10b) and suggests a current phase of relative quiescence in comparison, for instance, to the period prior to 1750.

5.4. Comparison with present-day geodetic deformation

Finally, we compare the seismological results with present-day

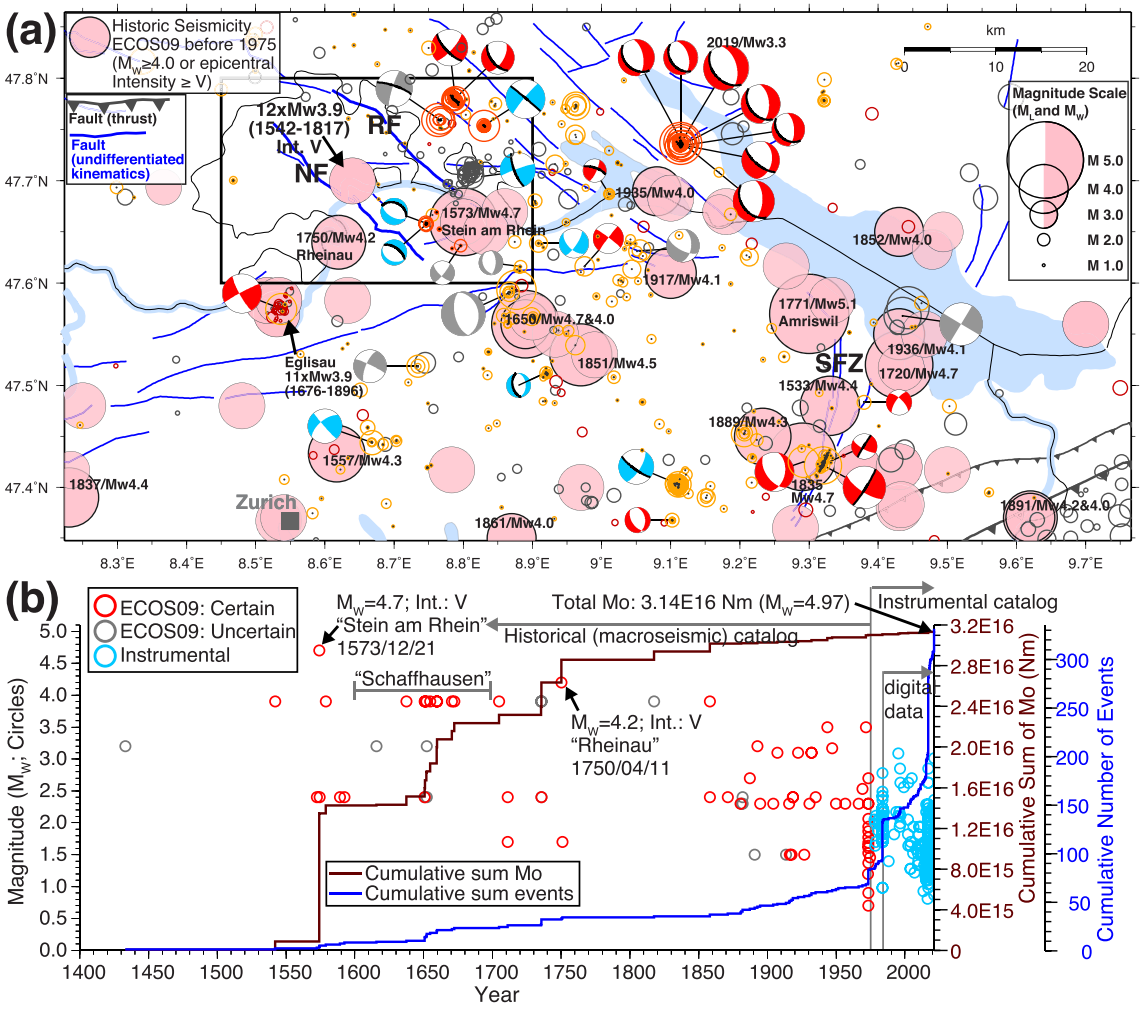

Fig. 10. Comparison between instrumental and historical seismicity in the region of the Hegau-Bodensee Graben (HBG). (a) Instrumental seismicity (open circles; size indicates local magnitude M_L as shown in the legend) and corresponding focal mechanisms as displayed in Fig. 3. Pink circles labeled with year and moment magnitude (M_W) indicate historical earthquakes with $M_W \geq 4.0$ included in the ECOS-09 catalog (Fäh et al., 2011). Additional pink circles indicate historical events with $M_W < 4.0$ and intensities $\geq$ V on the European Macroseismic Scale (EMS-98; Grünthal, 1998). Size of the pink circles indicates M_W as shown in the legend. See caption of Fig. 1 for references of shown fault traces. NF: Neuhausen Fault; RF: Randen Fault; SFZ: St. Gallen Fault Zone. (b) M_W and cumulative sum of the seismic moment (M_0) as well as number of earthquakes in the southwestern part of the HBG (region outlined by box in (a)) from historical ECOS-09 and instrumental catalogs of the SED. For the instrumental catalog, local magnitudes (M_L) were converted to M_W using the scaling relationship of Goertz-Allmann et al. (2011). (For interpretation of the references to colour in this figure legend, the reader is referred to the web version of this article.)

vertical and horizontal deformation rates derived from geodetic datasets across the graben. Background colors in Fig. 11a show interpolated vertical uplift rates derived from high-precision levelling data acquired by various campaigns since 1903 (Schlatter, 2007; Schlatter, 2014). The reference benchmark of the levelling data is located in Aarburg, Switzerland (47.32049°N/7.89900°E; Schlatter, 2007, Schlatter, 2014). Vertical deformation rates in the region of the graben relative to the reference benchmark are small and range between −0.1 and +0.1 mm/yr. These amplitudes are close to, or smaller than the noise level of the levelling data in this region (Schlatter, 2007, Schlatter, 2014). In addition, this levelling data cover only the SW boundary of the graben and relative changes across the graben cannot be reliably resolved. Likewise, no clear relative changes across the graben are observable in the levelling data of Fuhrmann et al. (2014), which cover the NW part of the graben in southern Germany (not shown). We therefore conclude that the vertical surface deformation of the graben is not resolved with the current levelling data and absolute rates are likely <0.1–0.2 mm/yr.

Arrows in Fig. 11a indicate horizontal deformation rates (velocities) as provided by the Swiss national reference system (CHTRF2016) for permanent and campaign GNSS stations in northern Switzerland. All velocities are relative to the GNSS station Zimmerwald (ZIMM, 46.877095°N/7.465273°E), located about 8 km south of Bern (e.g., Brockmann et al., 2012). For the permanent stations, we compared the CHTRF2016 velocities with a more recent solution (2021.8), which includes five years of additional data. The corresponding absolute velocities in Fig. 11b and Table S1 indicate about 30% lower velocities for stations TRLK and THYN (as well as reduced uncertainties) for the recent 2021.8 solution. This comparison suggests that GNSS velocities are currently still overestimated and velocities will likely further decrease with additional observation time.

Our analysis is focused on the relative velocity v_{TT} across the Neuhausen and Randen Faults derived from the two high-quality NaGNet (Nagra, 2014) stations TRLK (located on the footwall of the Neuhausen Fault) and THYN (located on the hanging wall of the Randen Fault; see Fig. 11b and c). For this analysis, we use the 2021.8 solution, since it is based on a longer observation period and therefore provides statistically more significant geodetic information to study cumulative slip rates for the SW flank of the graben.

We estimate the relative velocity v_{TT} to be 0.09 mm/yr. The vector v_{TT} can be further decomposed into a strike-parallel (v_{Nhsp} = 0.06 mm/

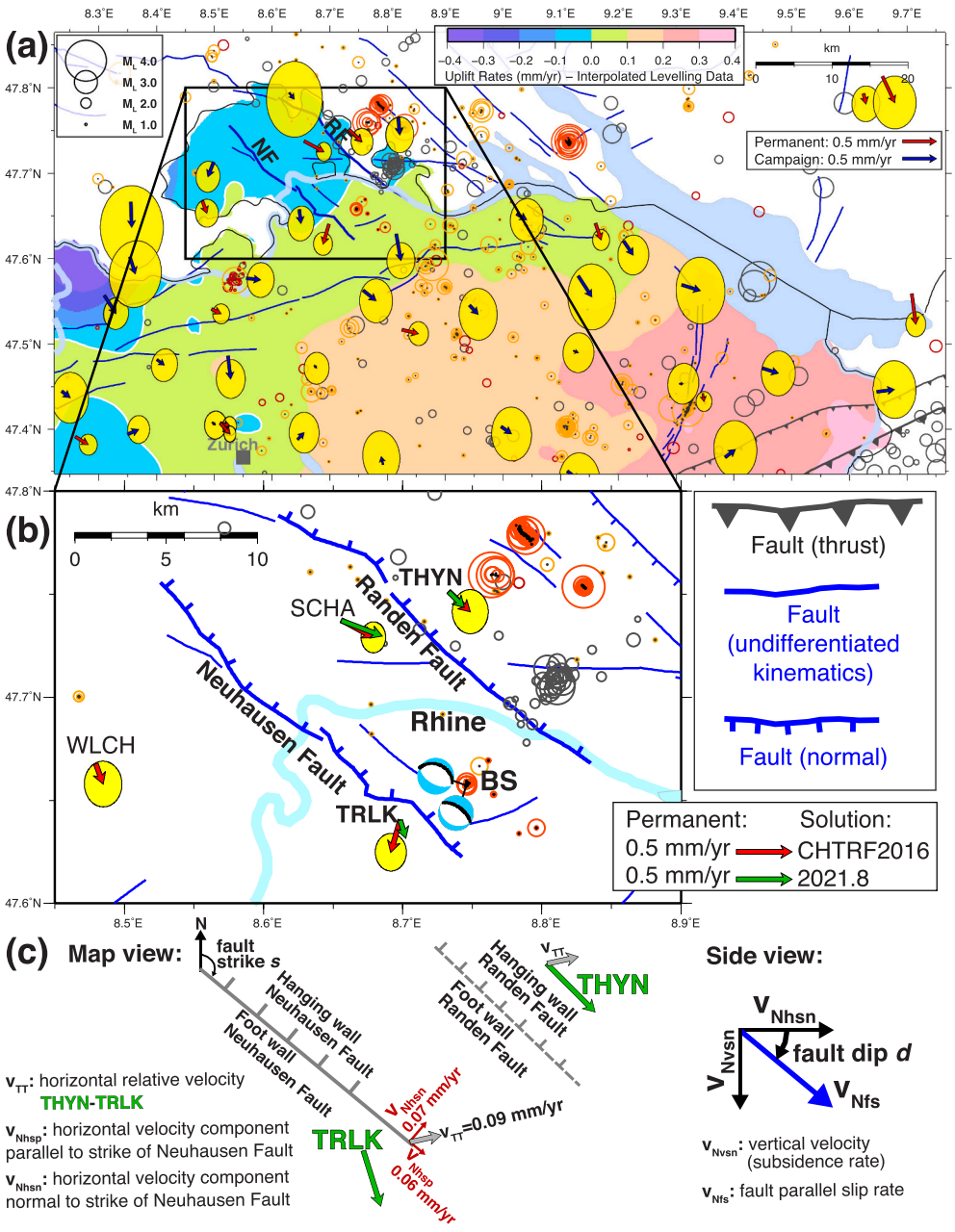

Fig. 11. Instrumental seismicity, geodetic deformation rates and slip-rate estimates for the major boundary faults of the Hegau-Bodensee Graben. (a) Map with interpolated vertical deformation rates from levelling data (Schlatter, 2007, Schlatter, 2014; background colors) and horizontal deformation rates (CHTRF2016 solution) of permanent and campaign GNSS sites (arrows). Yellow ellipses indicate the estimated horizontal uncertainties of the GNSS velocities. All GNSS velocities are relative to the GNSS station Zimmerwald located about 8 km south of Bern. See caption of Fig. 1 for references of shown fault traces. (b) Blow-up of (a), including the Neuhausen and Randen Faults at the southwestern edge of the graben. Additional green arrows indicate the horizontal velocities of the more recent 2021.8 solution for permanent stations TRLK, THYN, SCHA. BS: Basadingen-Schlattingen microearthquake sequence. (c) Conceptual sketch summarizing horizontal velocities of the 2021.8 solution across the Neuhausen and Randen Faults (green arrows) and slip-rate estimates calculated from the relative velocity v_{TT} between station THYN and TRLK (gray arrow). See text for further details. (For interpretation of the references to colour in this figure legend, the reader is referred to the web version of this article.)

yr) and strike-normal (v_{Nhsn} = 0.07 mm/yr) component with respect to the strike of the Neuhausen Fault (Fig. 11c). The relative velocity v_{TT} therefore consists of a dextral and a normal (extensional) deformation component across the two faults, consistent with the transtensional regime indicated by the focal mechanisms in Figs. 3 and 9.

The fault parallel slip rate v_{Nfs} on a normal fault dipping at an angle d (Fig. 11c) can be calculated from:

$$v_{Nfs} = \frac{v_{Nhsn}}{cosd}.$$

Assuming a fault dip d of about 60°, as indicated by our interpretation in Fig. 5b, would result in cumulative slip rates on the order of 0.14 mm/yr, or 0.07 mm/yr assuming an even split between the Neuhausen and Randen Faults. In turn, such fault slip would result in a vertical subsidence rate $v_{Nvsn} = \tan(d) \bullet v_{Nhsn}$ of the hanging-wall block of the Neuhausen and Randen Faults (Fig. 11c) of 0.06 mm/yr.

While these rates appear rather small, slip on the order of 0.07 m could be accumulated on such normal fault over a 1000-year period. According to the empirical relationships of Wells and Coppersmith (1994) between displacement (either maximum or average value) on normal faults and M_W, such slip would be sufficient for a magnitude M_W 5.8–6.0 earthquake, if released in a single rupture on a single fault. This M_W estimate, however, is rather uncertain because of the sparse number of observations of displacements <0.1 m in the dataset of Wells and Coppersmith (1994) and the considerable scatter of M_W values (on the order of one magnitude) in this range. Alternative earthquake-scaling relationships based on geodetic observations (Brengman et al., 2019) estimate M_W values on the order of 5.0–5.3 for a slip of 0.07 m. Bohnhoff et al. (2009) associate displacements of 0.04–0.4 m with "moderate" earthquakes (magnitudes 4.0–6.0). The maximum magnitude reported in the historical earthquake catalog within the southwestern edge of the graben (area in Fig. 11b) over the past 600 years is only M_W = 4.7 (slip on the order of 0.02–0.03 m according to the regression of Wells and Coppersmith, 1994 for normal faults) and the total sum of the seismic moment M_0 released in the same period corresponds to an M_W = 5

earthquake only (Fig. 10b). However, uncertainties related to the regression of Wells and Coppersmith (1994) as described above, the incompleteness of the historical earthquake catalog and the geodetic velocity estimates that lead to overestimated slip rates are too large to conclusively interpret this apparent deficit in seismic moment release. On the scale of one million years, a slip rate of 0.07 mm/yr would result in vertical offsets on the order of 60 m on the Neuhausen or Randen normal faults. Although this offset is in the range of the maximum total offsets observed for the Randen (about 250 m) and Neuhausen (about 100 m) Faults (e.g., Müller et al., 2002), it is not in line with geomorphological and Quaternary geological field observations along the Randen and Neuhausen Faults (e.g., Hofmann, 1981).

Overall, the above-outlined inconsistencies question the extrapolation of small geodetic deformation-rate measurements to geological timescales. Furthermore, the deformation might be accommodated by additional structures or faults might not be entirely locked during interseismic phases. The spatial resolution of the GNSS network as well as the signal-to-noise level of the current geodetic data, however, is not sufficient to resolve these questions. Nevertheless, magnitudes of historical earthquakes indicate that slip rates have the potential to generate moderate-sized earthquakes up to $M_W = 5$ in the Hegau-Lake Constance region on timescales of several hundred years. This estimate is in agreement with the one of Fabbri et al. (2021), who suggested a similar M_W range of 4.3–4.8 based on dimensions of faults imaged within Lake Constance. Considering timescales of several thousand years and longer, accumulated slip as well as fault dimensions, for instance, of the Neuhausen or Randen Faults (length and width as indicated in Figs. 3 and 4) might be sufficient for magnitudes >5. Because of sparse data as well as poor physical understanding, estimating the maximum magnitude M_{max} in the context of probabilistic seismic hazard assessment (PSHA) studies is one of the most uncertain parameters, especially in regions of low strain rates and low-to-moderate seismicity such as Switzerland and southern Germany (e.g., Coppersmith et al., 2009; Wiemer et al., 2009; Holschneider et al., 2014). Typically, this estimate is based on analog areas from around the world and on estimates on fault length. It should be noted that the reference time of a typical maximum possible earthquake in low-seismicity areas are very long, up to 100,000 or 1 Mio. years (e.g., Wiemer et al., 2009). According to PSHA studies, magnitudes on the order of 5.5–7.0 are considered plausible scenarios in the Hegau-Lake Constance region on such timescales (e.g., Coppersmith et al., 2009; Burkhard and Grünthal, 2009; Wiemer et al., 2016 with references therein).

5.5. Comparison with the Upper Rhine Graben

Herein, we provide a short comparison of our findings for the HBG with the situation in the westward-adjacent Upper Rhine Graben (Fig. 1, hereafter referred to as URG), whose seismotectonic characterization is far more advanced (e.g., Bonjer et al., 1984; Lopes Cardozo and Granet, 2003; Barth et al., 2015). Present-day horizontal deformation rates in the Hegau-Lake Constance region appear to be not significantly different from values observed in the source region of the 1356 M_W 6.7–7.1 earthquake of Basel, which is located at the southern end of the URG (Fig. S5). This raises the question of how strain is distributed between the two graben systems and about the likelihood for $M_W > 5$ earthquakes in the Hegau-Lake Constance region on timescales of thousand years and more. In comparison, present-day subsidence rates (including sediment compaction) in the URG derived from geodetic data are on the order of 0.2–0.5 mm/yr (Fuhrmann et al., 2014). Nivière et al. (2008) estimated maximum vertical fault slip rates on the eastern side of the URG near Freiburg of 0.04–0.18 mm/yr during Quaternary times (for a summary on deformation rates see also Barth et al., 2015 with references therein). Although still small in absolute sense, relative subsidence rates across the URG are higher compared to our estimates derived for the HBG. This difference is also in agreement with strain maps of Sánchez et al. (2018), also implying relatively higher strain rates in the vicinity of the URG compared to the Hegau-Lake Constance region. The higher deformation rates are in line with the abundant observation of distinct geomorphological features on either side of the URG (e.g., Nivière et al., 2008) as well as its relatively higher seismic activity, particularly in terms of seismic moment release (Fig. S6). The b-values derived from frequency-magnitude distributions of recent instrumental seismicity in the period 2000–2021, however, show no significant differences between both regions (Fig. S7). In summary, our comparison suggests that the URG, as a major segment of the European Cenozoic Rift System (Dèzes et al., 2004), is the dominant weak zone in the northern Alpine foreland, accumulating relatively more strain in the present-day stress field compared to the HBG. In contrast to the URG, we therefore consider the occurrence of $M_W > 5$ earthquakes on timescales of thousand years in the Hegau-Lake Constance region to be less likely. This conclusion is in line with the average probabilistic return period of $M \geq 6.5$ earthquakes reported in the *Seismic Hazard Model 2015 for Switzerland* (Wiemer et al., 2016). Within the Basel region this return period is on the order of 3000 years, while it is on the order of 6000–8000 years within the Hegau-Lake Constance region.

6. Conclusions

Significant improvements of the seismic network in the border region between northern Switzerland and southern Germany over the last 10 years allowed the identification and high-resolution imaging of seismically active faults associated with the Hegau-Bodensee Graben located in the northern foreland of the Central Alps. Our results contribute to an improved seismotectonic characterization of the slowly deforming graben and provide information for a refined seismic hazard assessment in future. The key findings of this study are that (1) bounding faults on either side of the graben show indications for present-day seismic activity. Most of the imaged structures, however, cannot be reliably associated with previously mapped faults and have no obvious geomorphological surface expression, likely due to poor outcrop conditions; (2) bounding faults root in the crystalline basement, possibly affecting deep parts of the crust down to 20 km depth; (3) the NW-SE striking bounding faults appear favorably to optimally oriented to be reactivated in a dextral transtensional sense in the present-day stress field. Slip rates across the Neuhausen and Randen Faults estimated from relative horizontal velocities of permanent GNSS stations are likely <0.1 mm/yr. In comparison with historical seismicity over the past 600 years and geomorphic field observations, geodetic rates of 0.1 mm/yr appear overestimated. Nevertheless, magnitudes of historical earthquakes indicate that slip rates have the potential to generate moderate-sized earthquakes up to $M_W = 5$ in the Hegau-Lake Constance region on timescales of several hundred years.

CRediT authorship contribution statement

Tobias Diehl: Conceptualization, Methodology, Formal analysis, Software, Visualization, Writing – original draft. **Herfried Madritsch:** Conceptualization, Visualization, Writing – original draft. **Michael Schnellmann:** Conceptualization, Writing – review & editing, Project administration. **Thomas Spillmann:** Writing – review & editing, Resources. **Elmar Brockmann:** Writing – review & editing, Resources, Data curation. **Stefan Wiemer:** Writing – review & editing, Project administration.

Declaration of Competing Interest

The authors declare the following financial interests/personal relationships which may be considered as potential competing interests:

Tobias Diehl reports financial support was provided by Nationale Genossenschaft für die Lagerung radioaktiver Abfälle (Nagra).

Data availability

The majority of seismic data used in this study was recorded by permanent and temporary seismic networks in Switzerland (network codes CH, 8D; Swiss Seismological Service (SED) At ETH Zurich, 1983, Swiss Seismological Service (SED) at ETH Zurich, 2005), southern Germany (network codes LE, GR; Landeserdbebendienst Baden-Wuerttemberg, Regierungspraesidium Freiburg, 2009; Federal Institute for Geosciences and Natural Resources, 1976), Austria (network code OE; ZAMG - Zentralanstalt für Meterologie und Geodynamik, 1987), and France (RESIF, 1995). Waveform data from the SED permanent seismic network (network code CH) as well as the majority of waveform data collected by collaborating networks in the region are openly available through the European Integrated Data Archive (EIDA): http://www.orfeus-eu.org/data/eida/. Waveform data collected by temporary networks in Switzerland in the framework of Ph.D. studies or in collaboration with industry might be restricted or embargoed. The merged earthquake catalog with relocated earthquakes as well as the catalog with focal mechanisms presented in this study are provided in a permanent data repository (https://doi.org/10.3929/ethz-b-000575883). The digital elevation models shown in the manuscript and the supplementary material are based on the Shuttle Radar Topography Mission (SRTM) 1 Arc-Second Global elevation data (https://doi.org/10.5066/F7PR7TFT).

Acknowledgements

Comments by Klaus Reicherter and Hans Agurto-Detzel helped to improve the manuscript and are thankfully acknowledged. Furthermore, we thank Stefan Schmid, Angela Landgraf and Donat Fäh for helpful discussions and additional comments. In particular, we acknowledge the collaboration with our colleagues at the Landeserdbebendienst Baden-Württemberg in Freiburg (LED) and we thank Stefan Stange (LED) for providing us data of a temporary station in Hilzingen, which were crucial for determining well-constrained focal depths and focal mechanism of the Hilzingen sequence. Financial support from the Nationale Genossenschaft für die Lagerung radioaktiver Abfälle (Nagra) for the operation of several stations in northern Switzerland and the research presented in this study is gratefully acknowledged. We thank SwissEnergy (http://www.energieschweiz.ch) and the Swiss Federal Office of Energy (www.bfe.admin.ch) for the financial support of projects GEOBEST-CH/2 and SIAMIS-GT that provided the seismic instrumentation for various temporary monitoring networks in northern Switzerland. St. Galler Stadtwerke (sgsw) are gratefully acknowledged for their financial and logistic support for the St. Gallen monitoring network. We also thank Toni Kraft for his support with the Eglisau and other monitoring networks and his contributions to microseismic event detection in northern Switzerland.

Appendix A. Supplementary data

Supplementary data to this article can be found online at https://doi.org/10.1016/j.tecto.2022.229659.

References

Aki, K., Richards, P.G., 2002. Quantitative Seismology, 2nd ed. Published by University Science Books. ISBN 0-935702-96-2. 704pp.

Allenbach, R., Baumberger, R., Kurmann, E., Michael, C.S., Reynolds, L., 2017. GeoMol: Geologisches 3D-Modell des Schweizer Molassebeckens – Schlussbericht. Swisstopo, Wabern, p. 128p.

Baer, M., Deichmann, N., Fäh, D., Kradolfer, U., Mayer-Rosa, D., Rüttener, E., Schler, T., Sellami, S., Smit, P., 1997. Earthquakes in Switzerland and surrounding regions during 1996. Eclogae Geol. Helv. 90 (3), 557–567.

Barth, A., Ritter, J., Wenzel, F., 2015. Spatial variations of earthquake occurrence and coseismic deformation in the Upper Rhine Graben, Central Europe. Tectonophysics 651-652, 172–185. https://doi.org/10.1016/j.tecto.2015.04.004.

Birkhäuser, P., Roth, P., Meier, B., Naef, H., 2001. 3D-Seismik: Räumliche Erkundung der mesozoischen Sedimentschichten im Zürcher Weinland. Nagra. Technical Report, NTB 00-03, Nagra, Wettingen.

Bohnhoff, M., Dresen, G., Ellsworth, W.L., Ito, H., 2009. Passive seismic monitoring of natural and induced earthquakes: Case studies, future directions and socio-economic relevance. In: Cloetingh, S., Negendank, J. (Eds.), New Frontiers in Integrated Solid Earth Sciences. International Year of Planet Earth. Springer, Dordrecht. https://doi.org/10.1007/978-90-481-2737-5_7.

Bonjer, K.-P., Gelbke, C., Gilg, B., Rouland, D., Mayer-Rosa, D., Massinon, B., 1984. Seismicity and dynamics of the Upper Rhinegraben. J. Geophys. 55, 1–12.

Braile, L.W., Hinze, W.J., Keller, G.R., Lidiak, E.G., Sexton, J.L., 1986. Tectonic development of the New Madrid rift complex, Mississippi embayment, North America. Tectonophysics 131, 1–21. https://doi.org/10.1016/0040-1951(86)90265-9.

Brengman, C.M.J., Barnhart, W.D., Mankin, E.H., Miller, C.N., 2019. Earthquake-scaling relationships from geodetically derived slip distributions. Bull. Seismol. Soc. Am. 109 (5), 1701–1715. https://doi.org/10.1785/0120190048.

Brockmann, E., 2018. LV95 / CHTRF2016 (Swiss Terrestrial Reference Frame 2016): Teil 2: Auswertung der GNSS-Messungen 2016 und Resultate der Gesamtausgleichung. Report 16-19, Wabern.

Brockmann, E., Ineichen, D., Marti, U., Schaer, S., Schlatter, A., Villiger, A., 2012. Determination of tectonic movements in the Swiss Alps using GNSS and levelling. In: Geodesy for Planet Earth. Springer, Berlin, Heidelberg, pp. 689–695. https://doi.org/10.1007/978-3-642-20338-1_85.

Brockmann, E., Lutz, S., Zurutuza, J., Caporali, A., Lidberg, M., Völksen, C., Sánchez, L., Serpelloni, E., Bitharis, S.I., Pikridas, C., Fotiou, A., Mathis, E., Sánchez Sobrino, J. A., De Vargas, M. Valdés Péres, Vernant, P., Baron, A., Westerhaus, M., Legrand, J., Kreemer, C., Gianniou, M., Nykiel, G., Figurski, M., Kenyeres, A., Kurt, Ali Ihsan, 2019. Towards a Dense Velocity Field in Europe as a Basis for Maintaining the European Reference Frame, 27th IUGG Assembly, Montreal, July 8–18, 2019.

Burkhard, M., Grünthal, G., 2009. Seismic source zone characterization for the seismic hazard assessment project PEGASOS by the Expert Group 2 (EG1b). Swiss J. Geosci. 102, 149–188. https://doi.org/10.1007/s00015-009-1307-3.

Clinton, J., Cauzzi, C., Fäh, D., Michel, C., Zweifel, P., Olivieri, M., Cua, G., Haslinger, F., Giardini, D., 2011. The current state of strong motion monitoring in Switzerland, in Earthquake Data in Engineering Seismology: Predictive Models, Data Management and Networks (Geotechnical, Geological and Earthquake Engineering), Akkar, S., Gülkan, P., and van Eck, T., ISBN 10: 9400701519 | 2011.

Coppersmith, K.J., Youngs, R.R., Sprecher, C., 2009. Methodology and main results of seismic source characterization for the PEGASOS Project, Switzerland. Swiss J. Geosci. 102, 91–105. https://doi.org/10.1007/s00015-009-1309-1.

Deichmann, N., 1992. Structural and rheological implications of lower-crustal earthquakes below Northern Switzerland. Phys. Earth Planet. Inter. 69, 270–280.

Deichmann, N., Ballarin Dolfin, D., Kastrup, U., 2000a. Seismizität der Nord- und Zentralschweiz. *Nagra Technischer Bericht*. NTB 00-05,. Nagra, Wettingen.

Deichmann, N., Baer, M., Braunmiller, J., Dolfin, D.B., Bay, F., Delouis, B., Fäh, D., Giardini, D., Kastrup, U., Kind, F., Kradolfer, U., Kunzle, W., Rothlisberger, S., Schler, T., Salichon, J., Sellami, S., Spuhler, E., Wiemer, S., 2000b. Earthquakes in Switzerland and surrounding regions during 1999. Eclogae Geol. Helv. 93, 395–406.

Dèzes, P., Schmid, S.M., Ziegler, P.A., 2004. Evolution of the European Cenozoic Rift System: interaction of the Alpine and Pyrenean orogens with their foreland lithosphere. Tectonophysics 389 (1–2), 1–33. https://doi.org/10.1016/j.tecto.2004.06.011.

Diebold, P., Naef, H., Ammann, M., 1991. Zur Tektonik der zentralen Nordschweiz. Interpretation aufgrund regionaler Seismik, Oberflächengeologie und Tiefbohrungen. Nagra Tech. Ber. NTB 90–04. Nagra, Wettingen.

Diehl, T., Deichmann, N., Clinton, J., Husen, S., Kraft, T., Plenkers, K., Edwards, B., Cauzzi, C., Michel, C., Kästli, P., Wiemer, S., Haslinger, F., Fäh, D., Kradolfer, U., Woessner, J., 2013. Earthquakes in Switzerland and surrounding regions during 2012. Swiss J. Geosci. 106, 543–558. https://doi.org/10.1007/s00015-013-0154-4.

Diehl, T., Clinton, J., Kraft, T., Husen, S., Plenkers, K., Guilhelm, A., Behr, Y., Cauzzi, C., Kaestli, P., Haslinger, F., Faeh, D., Michel, C., Wiemer, S., 2014. Earthquakes in Switzerland and surrounding regions during 2013. Swiss J. Geosci. 107, 359–375. https://doi.org/10.1007/s00015-014-0171-y.

Diehl, T., Kraft, T., Kissling, E., Wiemer, S., 2017. The induced earthquake sequence related to the St. Gallen deep geothermal project (Switzerland): Fault reactivation and fluid interactions imaged by microseismicity. J. Geophys. Res. Solid Earth 122. https://doi.org/10.1002/2017JB014473.

Diehl, T., Clinton, J., Deichmann, N., Cauzzi, C., Kästli, P., Kraft, T., Molinari, I., Böse, M., Michel, C., Hobiger, M., Haslinger, F., Fäh, D., Wiemer, S., 2018. Earthquakes in Switzerland and surrounding regions during 2015 and 2016. Swiss J. Geosci. 111, 221–244. https://doi.org/10.1007/s00015-017-0295-y.

Diehl, T., Clinton, J., Cauzzi, C., Kraft, T., Kästli, P., Deichmann, N., Massin, F., Grigoli, F., Molinari, I., Böse, M., Hobiger, M., Haslinger, F., Fäh, D., Wiemer, S., 2021a. Earthquakes in Switzerland and surrounding regions during 2017 and 2018. Swiss J. Geosci. 114, 4. https://doi.org/10.1186/s00015-020-00382-2.

Diehl, T., Kissling, E., Herwegh, M., Schmid, S., 2021b. Improving absolute hypocenter accuracy with 3-D Pg and Sg body-wave inversion procedures and application to earthquakes in the Central Alps region. J. Geophys. Res. Solid Earth, 126. https://doi.org/10.1029/2021JB022155 e2021JB022155.

Egli, D., Mosar, J., Ibele, T., Madritsch, H., 2017. The role of precursory structures on Tertiary deformation in the Black Forest—Hegau region. Int. J. Earth Sci. (Geol. Rundsch.) 106, 2297–2318. https://doi.org/10.1007/s00531-016-1427-8.

Eisbacher, G.H., Lüschen, E., Wickert, F., 1989. Crustal-scale thrusting and extension on the Hercynian Schwarzwald and Vosges, Central Europe. Tectonics 8 (1−21). https://doi.org/10.1029/TC008i001p00001.

Fabbri, S.C., Affentranger, C., Krastel, S., Lindhorst, K., Wessels, M., Madritsch, H., Allenbach, R., Herwegh, M., Heuberger, S., Wielandt-Schuster, U., Pomella, H., Schwestermann, T., Anselmetti, F.S., 2021. Active faulting in Lake Constance

(Austria, Germany, Switzerland) unraveled by multi- vintage reflection seismic data. Front. Earth Sci. 9:670532 https://doi.org/10.3389/feart.2021.670532.
Fäh, D., Gisler, M., Jaggi, B., Kästli, P., Lutz, T., et al., 2009. The 1356 Basel earthquake: an interdisciplinary revision. Geophys. J. Int. 178, 351–374. https://doi.org/10.1111/j.1365-246X.2009.04130.x.
Fäh, D., Giardini, D., Kästli, P., Deichmann, N., Gisler, M., Schwarz-Zanetti, G., Alvarez-Rubio, S., Sellami, S., Edwards, B., Allmann, B., Bethmann, F., Woessner, J., Gassner-Stamm, G., Fritsche, S., Eberhard, D., 2011. ECOS-09 Earthquake Catalogue of Switzerland Release 2011 Report and Database, Public Catalogue, 17. 4. 2011. Swiss Seismological Service ETH Zurich, Report SED/RISK/R/001/20110417.
Federal Institute for Geosciences and Natural Resources, 1976. German Regional Seismic Network (GRSN). Bundesanstalt für Geowissenschaften und Rohstoffe. https://doi.org/10.25928/MBX6-HR74.
Fuhrmann, T., Westerhaus, M., Zippelt, K., et al., 2014. Vertical displacement rates in the Upper Rhine Graben area derived from precise leveling. J. Geod. 88, 773–787. https://doi.org/10.1007/s00190-014-0721-0.
Goertz-Allmann, B.P., Edwards, B., Bethmann, F., Deichmann, N., Clinton, J., Fäh, D., Giardini, D., 2011. A new empirical magnitude scaling relation for Switzerland. Bull. Seismol. Soc. Am. 101, 3088–3095. https://doi.org/10.1785/0120100291.
Grünthal, G., 1998. European Macroseismic Scale 1998 (EMS-98). Cahiers du Centre Européen de Géodynamique et de Séismologie 15, Centre Européen de Géodynamique et de Séismologie, Luxembourg, 99 pp.
Hardebeck, J.L., Michael, A.J., 2006. Damped regional-scale stress inversions: methodology and examples for southern California and the Coalinga aftershock sequence. J. Geophys. Res. Solid Earth 111, B11310. https://doi.org/10.1029/2005JB004144.
Hardebeck, J.L., Shearer, P.M., 2002. A new method for determining first-motion focal mechanisms. Bull. Seismol. Soc. Am. 92, 2264–2276.
Heuberger, S., Roth, P., Zingg, O., Naef, H., Meier, B.P., 2016. The St. Gallen Fault Zone: a long-lived, multiphase structure in the North Alpine Foreland Basin revealed by 3D seismic data. Swiss J. Geosci. 109 (1), 83–102. https://doi.org/10.1007/s00015-016-0208-5.
Hofmann, F., 1981. Geologischer Atlas 1:25′000 Blatt Neunkirch (LK1031). Swisstopo, Wabern.
Holschneider, M., Zöller, G., Clements, R., Schorlemmer, D., 2014. Can we test for the maximum possible earthquake magnitude? J. Geophys. Res. Solid Earth 119, 2019–2028. https://doi.org/10.1002/2013JB010319.
Homewood, P., Allen, P.A., Williams, G.D., 1986. Dynamics of the Molasse Basin of western Switzerland. In: Allen, P.A., Homewood, P. (Eds.), Foreland Basins. Int Assoc. Sedimentol. Spec Publ, vol. 8, pp. 199–217.
Houlie, N., Woessner, J., Giardini, D., Rothacher, M., 2018. Lithosphere strain rate and stress field orientations near the Alpine arc in Switzerland. Sci. Rep. 8, 1–14. https://doi.org/10.1038/s41598-018-20253-z.
Husen, S., Kissling, E., Deichmann, N., Wiemer, S., Giardini, D., Baer, M., 2003. Probabilistic earthquake location in complex three-dimensional velocity models: application to Switzerland. J. Geophys. Res. 108 (B2), 2077–2096.
Ibele, T., 2015. Tectonics of the Hegau and Lake Constance Region: A Synthesis Based on Existing Literature. Nagra working report, NAB 12-23,. Nagra, Wettingen, p. 70.
Johnston, A.C., Schweig, E.S., 1996. The enigma of the New Madrid earthquakes of 1811-1812. Annu. Rev. Earth Planet. Sci. 24, 339–384. https://doi.org/10.1146/annurev.earth.24.1.339.
Kastrup, U., Zoback, M.-L., Deichmann, N., Evans, K., Giardini, D., Michael, A.J., 2004. Stress field variations in the Swiss Alps and the northern Alpine foreland derived from inversion of fault plane solutions. J. Geophys. Res. 109 (B1) https://doi.org/10.1029/2003JB002550B01402.
Kissling, E., Schlunegger, F., 2018. Rollback orogeny model for the evolution of the Swiss Alps. Tectonics 37, 1097–1115. https://doi.org/10.1002/2017TC004762.
Kraft, T., Mignan, A., Giardini, D., 2013. Optimization of a large-scale microseismic monitoring network in northern Switzerland. Geophys. J. Int. 195, 474–490. https://doi.org/10.1093/gji/ggt225.
Kraft, T., Herrmann, M., Diehl, T., 2016. Analysis of Induced Microseismicity at the Geothermal Project Schlattingen (Canton Thurgau, Switzerland). Nagra Project Report, NPB 16–12. Nagra, Wettingen.
Landeserdbebendienst Baden-Wuerttemberg, Regierungspraesidium Freiburg, 2009. Landeserdbebendienst Baden-Wuerttemberg [Data set]. International Federation of Digital Seismograph Networks. https://doi.org/10.7914/SN/LE.
Landgraf, A., Kübler, S., Hintersberger, E., Stein, S., 2017. Active tectonics, earthquakes and palaeoseismicity in slowly deforming continents. Geol. Soc. Lond., Spec. Publ. 432, 1–12. https://doi.org/10.1144/SP432.13.
Lanza, F., Diehl, T., Deichmann, N., Kraft, T., Nussbaum, C., Schefer, S., Wiemer, S., 2022. The Saint-Ursanne earthquakes of 2000 revisited: evidence for active shallow thrust-faulting in the Jura fold-and-thrust belt. Swiss J. Geosci. 115, 2. https://doi.org/10.1186/s00015-021-00400-x.
Lee, T., Diehl, T., Kissling, E., Wiemer, S., 2023. New insights into the Rhône–Simplon fault system (Swiss Alps) from a consistent earthquake catalogue covering 35 yr. Geophys. J. Int. 232 (3), 1568–1589. https://doi.org/10.1093/gji/ggac407.
Lippolt, H.J., Gentner, W., Wimmenauer, W., 1963. Altersbestimmungen nach der Kalium-Argon-Methode an tertiären Eruptivgesteinen Südwestdeutschlands. Jahreshefte des Geologischen Landesamts Baden-Württemberg, 6, pp. 507–538.
Lomax, A., Virieux, J., Volant, P., Thierry-Berge, C., 2000. Probabilistic earthquake location in 3D and layered models. In: Thurber, C.H., Rabinowitz, N. (Eds.), Advances in Seismic Event Location. Kluwer Academic Publishers, London, pp. 101–134.
Lomax, A., Michelini, A., Curtis, A., 2014. Earthquake location, direct, global-search methods. In: Meyers, R.A. (Ed.), Encyclopedia of Complexity and Systems Science. Springer, New York, pp. 1–33.
Lopes Cardozo, G.G.O., Granet, M., 2003. New insight in the tectonics of the southern Rhine Graben-Jura region using local earthquake seismology. Tectonics 22 (6), 1078. https://doi.org/10.1029/2002TC001442.
Mader, S., Ritter, J.R.R., Reicherter, K., the ALP ARRAY Working group, 2021. Seismicity and seismotectonics of the Albstadt Shear Zone in the northern Alpine foreland. Solid Earth 12 (6), 389–1409.
Madritsch, H., 2015. Outcrop-scale fracture systems in the Alpine foreland of central northern Switzerland: kinematics and tectonic context. Swiss J. Geosci. 108, 155–181. https://doi.org/10.1007/s00015-015-0203-2.
Madritsch, H., Naef, H., Meier, B., Franzke, H.J., Schreurs, G., 2018. Architecture and kinematics of the Constance–Frick Trough (Northern Switzerland): implications for the formation of post-Variscan basins in the foreland of the Alps and scenarios of their Neogene reactivation. Tectonics 37, 2197–2220. https://doi.org/10.1029/2017TC004945.
Malz, A., Madritsch, H., Meier, B., Kley, J., 2016. An unusual triangle zone in the external northern Alpine foreland (Switzerland): Structural inheritance, kinematics and implications for the development of the adjacent Jura fold-and-thrust belt. Tectonophysics 670, 127–143. https://doi.org/10.1016/j.tecto.2015.12.025.
Martínez-Garzón, P., Kwiatek, G., Ickrath, M., Bohnhoff, M., 2014. MSATSI: a MATLAB package for stress inversion combining solid classic methodology, a new simplified user-handling, and a visualization tool. Seismol. Res. Lett. 85, 896–904. https://doi.org/10.1785/0220130189.
Meghraoui, M., Delouis, B., Ferry, M., Giardini, D., Huggenberger, P., Spottke, I., Granet, M., 2001. Active normal faulting in the Upper Rhine Graben and paleoseismic identification of the 1356 Basel earthquake. Science 293, 2070–2073. https://doi.org/10.1126/science.1010618.
Michael, A.J., 1984. Determination of stress from slip data: faults and folds. J. Geophys. Res. Solid Earth 89, 11517–11526. https://doi.org/10.1029/JB089iB13p11517.
Mock, S., Herwegh, M., 2017. Tectonics of the central Swiss Molasse Basin: post-Miocene transition to incipient thick-skinned tectonics? Tectonics 36. https://doi.org/10.1002/2017TC004584.
Müller, G., Gees, R.A., 1968. Origin of the Lake Constance basin. Nature 217 (5131), 836–837. https://doi.org/10.1038/217836a0.
Müller, W.H., Naef, H., Graf, H.R., 2002. Geologische Entwicklung der Nordschweiz, Neotektonik und Langzeitszenarien Zürcher Weinland. Nagra Technical Report, NTB 99-08, Wettingen, p. 237.
Nagra, 2008. Vorschlag geologischer Standortgebiete für das SMA- und das HAA-Lager - Geologische Grundlagen Textband. Nagra Technischer Bericht NTB 08–04. Nagra, Wettingen.
Nagra, 2014. Vorschlag weiter zu untersuchender geologischer Standortgebiete mit zugehörigen Standortarealen für die Oberflächenanlage: Geologische Grundlagen. Technical Report NTB 14-02,. Nagra, Wettingen.
Nanjo, K., Schorlemmer, D., Woessner, J., Wiemer, S., Giardini, D., 2010. Earthquake detection capability of the Swiss Seismic Network. Geophys. J. Int. 181, 1713–1724.
Newman, A., Stein, S., Weber, J., Engeln, J., Mao, A., Dixon, T., 1999. Slow deformation and lower seismic hazard at the New Madrid seismic zone. Science 284, 619–621. https://doi.org/10.1126/science.284.5414.619.
Nivière, B., Bruestle, A., Bertrand, G., Carretier, S., Behrmann, J., Gourry, J.-C., 2008. Active tectonics of the southeastern Upper Rhine Graben, Freiburg area (Germany). Quat. Sci. Rev. 27 (5–6) https://doi.org/10.1016/j.quascirev.2007.11.018.
Pfiffner, O.A., 1986. Evolution of the north Alpine foreland basin in the Central Alps (Switzerland). In: Allen, P.A., Homewood, P. (Eds.), Foreland Basins. Blackwell Publishing Ltd., Oxford, pp. 219–228. https://doi.org/10.1002/9781444303810.ch11.
Plenkers, K., Husen, S., Kraft, T., 2015. A multi-step assessment scheme for seismic network site selection in densely populated areas. J. Seismol. 19 (4), 861–879. https://doi.org/10.1007/s10950-015-9500-5.
Poupinet, G., Ellsworth, W., Fréchet, J., 1984. Monitoring velocity variations in the crust using earthquake doublets: an application to the Calaveras Fault, California. J. Geophys. Res. Solid Earth 89, 5719–5731. https://doi.org/10.1029/JB089iB07p05719.
Reinecker, J., Schneider, G., 2002. Zur Neotektonik der Zollernalb: der Hohenzollerngraben und die Albstadt-Erdbeben. Jahresber. Mitt. Oberrhein Geol. Ver. 84, 391–417.
Reinecker, J., Tingay, M., Müller, B., Heidbach, O., 2010. Present-day stress orientation in the Molasse Basin. Tectonophysics 482, 129–138. https://doi.org/10.1016/j.tecto.2009.07.021.
RESIF, 1995. RESIF-RLBP French Broad-band network, RESIF-RAP strong motion network and other seismic stations in metropolitan France [Data set]. RESIF - Réseau Sismologique et géodésique Français. https://doi.org/10.15778/RESIF.FR.
Ring, U., Gerdes, A., 2016. Kinematics of the Alpenrhein-Bodensee graben system in the Central Alps: Oligocene/Miocene transtension due to formation of the Western Alps arc. Tectonics 35, 1367–1391. https://doi.org/10.1002/2015TC004085.
Roche, V., Childs, C., Madritsch, H., Camanni, G., 2020. Layering and structural inheritance controls on fault zone structure in three dimensions: a case study from the northern Molasse Basin, Switzerland. J. Geol. Soc. 28 https://doi.org/10.1144/jgs2019-052.
Sánchez, L., Völksen, C., Sokolov, A., Arenz, H., Seitz, F., 2018. Present-day surface deformation of the Alpine region inferred from geodetic techniques. Earth Syst. Sci. Data 10, 1503–1526.
Schaff, D., Bokelmann, G., Ellsworth, W., Zanzerkia, E., Waldhauser, F., Beroza, G., 2004. Optimizing correlation techniques for improved earthquake location. Bull. Seismol. Soc. Am. 94, 705–721. https://doi.org/10.1785/0120020238.
Schlatter, A., 2007. Das neue Landeshöhennetz der Schweiz LHN95, Geodätisch-geophysikalische Arbeiten in der Schweiz, Vol. 72. In: Schweizerische Geodätische Kommission / Swiss Geodetic Commission, Zürich. ISBN 978-3-908440-16-1.

Schlatter, A., 2014. Kinematische Gesamtausgleichung der Schweizer Landesnivellementlinien 2013 und Detaildarstellung der rezenten vertikalen Oberflächenbewegungen in der Zentralschweiz. Nagra working report, NAB 14-38. Nagra, Wettingen, p. 34.
Schneider, G., 1979. The earthquake in the Swabian Jura of 16 November 1911 and present concepts of seismotectonics. Tectonophysics 53, 279–288.
Schorlemmer, D., Woessner, J., 2008. Probability of detecting an earthquake. Bull. Seismol. Soc. Am. 98 (5), 2103–2217. https://doi.org/10.1785/0120070105.
Schreiner, A., 1992. Hegau und westlicher Bodensee. Geologische Karte von Baden-Württemberg 1:50 000, Erläuterungen, p. 290.
Sibson, R.H., 1990. Rupture nucleation on unfavorably oriented faults. Bull. Seismol. Soc. Am. 80, 1580–1604. https://doi.org/10.1029/JB090iB12p10223.
Singer, J., Diehl, T., Husen, S., Kissling, E., Duretz, T., 2014. Alpine lithosphere slab rollback causing lower crustal seismicity in northern foreland. Earth Planet Sci. Lett. 397, 42–56. https://doi.org/10.1016/J.Epsl.2014.04.002.
Stange, S., Brüstle, W., 2005. The Albstadt/Swabian Jura seismic source zone reviewed through the study of the earthquake of March 22, 2003. In: Jahresberichte und Mitteilungen des Oberrheinischen Geologischen Vereins, Band 87, pp. 391–414.
Stange, S., Hensch, M., Rodler, F.-A., Brüstle, W., 2017. Die Erdbebenserie im Hegau 2016/2017. Poster bei der 75. Jahrestagung der Deutschen Geophysikalischen Gesellschaft in Potsdam, 27.-30.3.2017.
Swiss Seismological Service (SED) At ETH Zurich, 1983. National Seismic Networks of Switzerland. ETH Zürich, 10.12686/sed/networks/ch.
Swiss Seismological Service (SED) at ETH Zurich, 2005. Temporary Deployments in Switzerland Associated with Aftershocks and Other Seismic Sequences. ETH Zurich. https://doi.org/10.12686/sed/networks/8d.
Swisstopo, 2005. Tektonische Karte der Schweiz 1:500,000. Federal Office of Topography Swisstopo, Wabern.
Villiger, A., 2014. Improvement of the Kinematic Model of Switzerland (Swiss 4D II). Ph. D. Thesis,. ETH Zürich. https://doi.org/10.3929/ethz-a-010163325.
von Hagke, C., Cederbom, C.E., Oncken, O., Stöckli, D.F., Rahn, M.K., Schlunegger, F., 2012. Linking the northern Alps with their foreland: the latest exhumation history resolved by low temperature thermochronology. Tectonics 31, TC5010. https://doi.org/10.1029/2011TC003078.
Waldhauser, F., Ellsworth, W.L., 2000. A double-difference earthquake location algorithm: method and application to the northern Hayward fault, California. Bull. Seismol. Soc. Am. 90, 1353–1368. https://doi.org/10.1785/0120000006.
Weber, J., Stein, S., Engeln, J., 1998. Estimation of intraplate strain accumulation in the New Madrid seismic zone from repeat GPS surveys. Tectonics 17, 250–266. https://doi.org/10.1029/97TC03550.
Wells, D.L., Coppersmith, K.J., 1994. New Empirical Relationships Among Magnitude, Rupture Length, Rupture Width, Rupture Area, and Surface Displacement, 84, pp. 974–1002.
Wiemer, S., Giardini, D., Fäh, D., et al., 2009. Probabilistic seismic hazard assessment of Switzerland: best estimates and uncertainties. J. Seismol. 13, 449–478. https://doi.org/10.1007/s10950-008-9138-7.
Wiemer, S., et al., 2016. Seismic Hazard Model 2015 for Switzerland (SUIhaz2015), Swiss Seismological Service at ETH Zurich, pp. 1–163. https://doi.org/10.12686/a2.
Willett, S.D., Schlunegger, F., 2010. The last phase of deposition in the Swiss Molasse Basin: from foredeep to negative-alpha basin. Basin Res. 22, 623–639. https://doi.org/10.1111/j.1365-2117.2009.00435.
Wimmenauer, W., 1974. The alkaline province of Central Europe and France. In: Sorensen, H. (Ed.), The Alkaline Rocks. Wiley, London, pp. 238–271.
ZAMG - Zentralanstalt für Meterologie und Geodynamik, 1987. Austrian seismic network [Data set]. International Federation of Digital Seismograph Networks. https://doi.org/10.7914/SN/OE.